1 **The impact of shipping, agricultural, and urban emissions on single particle chemistry**
2 **observed aboard the R/V Atlantis during CalNex**

3

4 Cassandra J. Gaston,[1‡]   Patricia K. Quinn,[2] Timothy S. Bates,[2] Jessica B. Gilman,[3] Daniel M. Bon,[3†]
5 William C. Kuster,[3] and Kimberly A. Prather[1,4*]

6

7 [1]Scripps Institution of Oceanography, University of California, San Diego, La Jolla, CA 92093 USA

8

9 [2]NOAA Pacific Marine Environmental Laboratory, Seattle, WA 98115 USA

10

11 [3]NOAA Earth System Research Laboratory, Boulder, CO 80305 USA and Cooperative Institute for
12 Research in Environmental Sciences, University of Colorado, Boulder, CO 80309

13

14 [4]Department of Chemistry and Biochemistry, University of California, San Diego, La Jolla, CA 92093-
15 0314 USA

16

17 [‡]Current Address: Department of Atmospheric Sciences, University of Washington, Seattle, WA 98195
18 USA

19

20 [†]Current Address: Planning and Policy Program, Air Pollution Control Division, Colorado Department
21 of Public Health and Environment, Denver, CO 80246 USA

22

23 *Corresponding author: kprather@ucsd.edu, 858-822-5312. Fax: 858-534-7042.

24

Abstract:

The CalNex field campaign was undertaken to obtain a better understanding of the regional impacts of different pollution sources in California. As part of this study, real-time shipboard measurements were made of the size-resolved single-particle mixing-state of sub- and super-micron particles (0.2-3.0 um aerodynamic diameter) along the California coast where major differences were noted between Southern and Northern California. In Southern California, particles containing soot made up the largest fraction of submicron particles (~38% on average and up to ~89% by number), whereas organic carbon (OC) particles comprised the largest fraction of submicron number concentrations (~29% on average and up to ~78% by number) in Northern California including the Sacramento area. The mixing-state of these carbonaceous particle types varied during the cruise with sulfate being more prevalent on soot-containing particles in Southern California due to the influence of fresh shipping and port emissions in addition to contributions from marine biogenic emissions. Contributions from secondary organic aerosol species, including amines, and nitrate were more prevalent in Northern California, as well as during time periods impacted by agricultural emissions (e.g., from the inland Riverside and Central Valley regions). These regional differences and changes in the mixing-state and sources of particles have implications for heterogeneous reactivity, water uptake, and cloud nucleating abilities for aerosols in California.

2

1. Introduction

Atmospheric aerosols contribute to air pollution, have adverse effects on human health, and perturb the Earth's radiative balance [*Poschl*, 2005]; both aerosol size and composition play key yet uncertain roles in these effects. One aim of the Research at the Nexus of Air Quality and Climate Change (CalNex) field campaign was to elucidate the links between aerosols, air pollution, and climate in order to guide policies regarding emission regulations in California. Diverse particle sources impact California including ships, vehicle exhaust, oil refineries, meat cooking, and animal husbandry and agricultural emissions. The Ports of Los Angeles (LA) and Long Beach (LB) are the busiest container ports in the United States, contributing high levels of ship and port emissions (e.g., diesel truck emissions, oil refinery emissions) to Southern California. Locations in inland Southern California (e.g., Riverside) and the Sacramento and San Joaquin Valley areas in Northern California are impacted by dairy farm and agricultural emissions leading to high mass concentrations of particulate matter that contain large fractions of secondary species [*Chen et al.*, 2007; *Chow et al.*, 2006a; *Docherty et al.*, 2008; *Grover et al.*, 2008; *Hughes et al.*, 2000; *Hughes et al.*, 2002; *Magliano et al.*, 1999; *Pastor et al.*, 2003; *Qin et al.*, 2012; *Sorooshian et al.*, 2008]. Further, biogenic emissions from forested regions such as the Sierra Nevada foothills and from marine biological activity along the California coast also contribute to the aerosol burden in California [*Creamean et al.*, 2011; *Gaston et al.*, 2010]. Assessing how these regional differences in particle sources and secondary reactions in California impact the physicochemical properties of aerosols represents a key step in fulfilling the goals of the CalNex field campaign.

Single-particle mass spectrometry is well-suited for providing the high temporal resolution and mass spectral fingerprints necessary for distinguishing diverse particle sources as

3

well as assessing the impact of atmospheric processing (e.g., gas-to-particle partitioning, heterogeneous reactions, etc.) on particle size and chemistry [*Pratt and Prather*, 2011; *Sullivan and Prather*, 2005]. Aerosol time-of-flight mass spectrometry (ATOFMS), a single-particle technique, has been successfully used for the source apportionment of particulate matter in California for almost fifteen years [*Ault et al.*, 2010; *Creamean et al.*, 2011; *Gaston et al.*, 2010; *Hughes et al.*, 2000; *Moffet et al.*, 2008b; *Noble and Prather*, 1996; *Pastor et al.*, 2003; *Pratt et al.*, 2009; *Pratt and Prather*, 2009; *Qin et al.*, 2012; *Toner et al.*, 2008; *Whiteaker et al.*, 2002]. Herein we present real-time measurements of single-particle composition and size using ATOFMS during the CalNex campaign onboard the R/V Atlantis sampling platform. Atmospheric measurements were made off the California coast, targeting specific sources, including the Ports of LA and LB, continental outflow from the LA Basin, and emissions from Northern California including the inland, Sacramento area. This paper describes the significant differences observed in single-particle mixing-state and sources between these regions. The implications of these findings are discussed.

2. Experimental

2.1 CalNex

Ambient aerosol and gas-phase measurements were made onboard the R/V Atlantis from May 14-June 8, 2010 as part of the CalNex 2010 field campaign ([*Ryerson et al.*, 2013]; http://www.esrl.noaa.gov/csd/calnex/; http://saga.pmel.noaa.gov/data). The ship traveled from San Diego to Sacramento and then back to the Port of San Francisco where the study ended. The cruise track is shown in Figure 1. The air in the aerosol sampling manifold was conditioned to $60 \pm 5\%$ relative humidity (RH) using a heated inlet. Insulated conductive tubing extending

4

91   from the heated inlet provided air to the instruments at flows of ~ 30 lpm [*Bates et al.*, 2004].

92   Meteorological parameters, aerosol properties, and gas-phase constituents such as radon, SO_2,

93   O_3, etc. were measured onboard the ship [*Quinn and Bates*, 2005]. Hydrocarbons, including

94   toluene and benzene, were quantified using gas chromatography equipped with a flame

95   ionization detector (GC-FID) [*Bon et al.*, 2011]. The ratio of toluene to benzene can be used

96   as an indicator of photo-chemical age [*Gelencser et al.*, 1997; *Roberts et al.*, 1984]. Air masses

97   containing fresh urban emissions that have undergone minimal photochemical processing

98   typically have toluene/benzene ratios ≥ 2, lower values are indicative of more photo-chemically

99   processed air masses as the more reactive toluene is preferentially removed by reactions with the

100 hydroxyl radical. Clean marine air masses are typically well-aged and are expected to have

101 toluene/benzene ratios <<1. Ship exhaust from the R/V Atlantis was filtered out by eliminating

102 time periods when the relative wind direction was aft of +100° (starboard) and -120° (port) off

103 the bow. All data presented here were filtered using this method. Data are presented in

104 coordinated universal time (UTC), which is 7 hours ahead of local time (PDT), as day of year

105 (DOY). For example, a date and time of 12:00 on January 1 presented in UTC would correspond

106 to DOY 1.5.

107 **2.2   Aerosol Measurements: ATOFMS**

108   The size-resolved chemical composition of individual aerosol particles from 0.2-3.0 um

109 aerodynamic diameter was measured in real-time using an aerosol time-of-flight mass

110 spectrometer (ATOFMS). The operating principles of the ATOFMS have been described

111 previously [*Gard et al.*, 1997; *Prather et al.*, 1994]. Briefly, particles are sampled through a

112 converging nozzle inlet into a differentially pumped vacuum chamber causing particles to be

113   accelerated to a size-dependent terminal velocity. Particles next enter the sizing region of the

114   instrument consisting of two continuous wave (532 nm) lasers separated by a fixed distance. The

115   time taken to traverse the laser beams is recorded giving the terminal velocity of the particle,

116   which is used to calculate the aerodynamic diameter of the particle. The particle velocity is also

117   used to time the firing of a Q-switched Nd:YAG laser (266 nm) operating at ~1.2 mJ laser power

118   that simultaneously desorbs and ionizes compounds from individual particles creating positive

119   and negative ions, which are analyzed in a dual polarity time-of-flight mass spectrometer.

120   Particle detection efficiencies are dependent on the ability of particles to interact with the 266 nm

121   radiation [*Dall'Osto et al.*, 2006; *Qin et al.*, 2006; *Wenzel et al.*, 2003]. Dual-polarity spectra

122   provide complementary information regarding the source (e.g., ships vs. sea salt) and age of the

123   particle (e.g., fresh vs. reacted sea salt) [*Guazzotti et al.*, 2001; *Noble and Prather*, 1996]. A lack

124   of negative ion spectra indicates the presence of tightly bound particle phase water, which

125   suppresses negative ions produced by laser desorption/ionization [*Neubauer et al.*, 1997;

126   *Neubauer et al.*, 1998]. Conditioning particles to 60% RH decreases some of this water, thus,

127   increasing the formation of negative ion spectra.

128   The YAADA software toolkit was used to import ion peak lists into MATLAB v 6.5.1

129   (The MathWorks, Inc.) for processing of ATOFMS data [*Allen*, 2002]. Single-particle mass

130   spectra were then analyzed using a clustering algorithm (ART-2a), which groups spectra together

131   with similar characteristics into distinct "clusters" [*Song et al.*, 1999]. These "clusters" are then

132   merged into distinct particle types based on the prevalent mass spectral ions and intensities,

133   which are indicative of particle sources and chemistry [*Noble and Prather*, 1996]. The

134   prevalence of these particle types were averaged into 1-hour time bins and separated into

135   submicron (0.2-1.0 um) and supermicron (1.0-3.0 um) particles. Each ion peak assignment

136   presented in this paper corresponds to the most likely ion produced at a given mass-to-charge

137   (*m/z*). Particle types described herein are defined by characteristic ion peaks and/or possible

138   sources and do not reflect all of the species present within a particular particle class.

3. Results

140   Temporal trends of single-particle measurements were analyzed to discern differences in

141   particle composition between sources in Southern and Northern California.   The temporal

142   variability of the most frequently observed particle types detected by ATOFMS as well as the

143   latitudinal position of the ship are shown in Figures 2a and 2b for sub- and super-micron

144   particles, respectively. Several trends in single-particle mixing-state were identified based on

145   differences in particle source, meteorological conditions, and aging processes. To illustrate this,

146   six distinct time periods are identified by colored boxes in Figure 2; the time periods are defined

147   as Riverside Transport (Period 1, boxed in red), Stagnant/Ports Transport (Period 2, boxed in

148   black), Marine/Coastal Transport (Period 3, boxed in cyan), Ports of Los Angeles/Long Beach

149   (LA/LB) (Period 4, boxed in green), Inland/Valley Transport (Period 5, boxed in orange), and

150   Bay Area/Sacramento (Period 6, boxed in purple). The following sections provide a detailed

151   comparison and discussion of the gas-phase species and meteorological conditions, prevalent

152   particle types and sources, the mixing-state of carbonaceous particles, and the secondary

153   particulate species present during each time period.

3.1   Characteristics of Each Period

155   During   the   Riverside,   Stagnant/Ports,   and   Marine/Coastal   Transport   periods,

156   measurements took place along the Southern California coast focusing on emissions from the LA

157　Basin, whereas measurements during the Ports of LA/LB period were entirely performed in the

158　Ports of LA and LB and surrounding shipping lanes. During the Inland/Valley Transport period,

159　measurements extended further north to include the Santa Barbara region; the Bay

160　Area/Sacramento period measurements were made in Northern California when the ship

161　remained in the Deep Water Channel/Sacramento region for 3 days. Table 1 shows the

162　corresponding dates and meteorological and gas phase measurements for each time period.

163　Figure 3 shows the 48-hour calculated air mass back trajectories at 500 m height [*Draxler and*

164　*Rolph*, 2011] for each time period to highlight differences in air mass transport conditions. The

165　Stagnant/Ports and Ports of LA/LB periods were heavily influenced by emissions from the Ports

166　of LA/LB while the Riverside, Stagnant/Ports, Inland/Valley, and Bay Area/Sacramento periods

167　were influenced by agricultural and urban emissions from Riverside and/or the Central Valley.

168　The Marine/Coastal Transport period was influenced by oceanic emissions and serves as a

169　background period.

170　**3.1.1　Period 1:　Riverside Transport**

171　　　During the Riverside Transport period, HYSPLIT analysis indicates that the sampled air

172　masses were transported from the Riverside and Imperial Valley regions before traversing the

173　port and Santa Monica regions (see Figure 3a). Thus, the Riverside Transport period is expected

174　to be influenced by urban, port, and agricultural emissions. Particulate matter in Riverside

175　typically is well-aged as indicated by high concentrations of secondary species such as nitrate,

176　amines, ammonium, and secondary organics [*Hughes et al.*, 2000; *Hughes et al.*, 2002; *Liu et al.*,

177　2000; *Pastor et al.*, 2003; *Pratt et al.*, 2009; *Pratt and Prather*, 2009; *Qin et al.*, 2012]. The ratio

178　of toluene to benzene was not available during this period; however, available NO_x/NO_y ratios

8

179   indicated that the air masses during this period were photo-chemically aged. The average radon

180   concentration was high (2500 ± 760 mBq/m^3) indicating that continentally influenced air masses

181   were sampled. The average temperature was low (13.2 ± 0.6°C) while RH was high ($89 \pm 3\%$).

3.1.2   Period 2: Stagnant/Ports Transport

183   Sampled air masses stagnated around the coast near the ports and Santa Monica region

184   during the Stagnant/Ports Transport period. Thus, port emissions (e.g., emissions from vehicles,

185   ships, etc.) contributed more significantly to the aerosol burden during the Stagnant/Ports

186   Transport than the Riverside Transport period. Some air masses also originated from the inland,

187   Central Valley area toward the end of the Stagnant/Ports Transport period potentially carrying

188   agricultural emissions. The lowest average toluene to benzene ratio, 0.4, was observed during

189   this period suggesting that air masses sampled during this period were heavily photo-chemically

190   aged. Again, high RH ($91 \pm 3\%$ on average) and low temperatures (13.4 ± 1.1°C) were

191   observed.

3.1.3   Period 3: Marine/Coastal Transport

193   During the Marine/Coastal Transport period, most air masses followed a northern

194   coastal/oceanic trajectory along the California coast. Wind speeds reached 14.5 m/s, which

195   enhanced the production of fresh sea spray particles from bursting bubbles generated by breaking

196   waves [*Blanchard and Woodcock*, 1957; *Monahan et al.*, 1983; *O'Dowd and De Leeuw*, 2007].

197   Thus, the Marine/Coastal Transport period is characterized by ocean-derived aerosol comprised

198   of both fresh sea salt and biogenic organics. This period is not necessarily representative of

199   clean marine conditions based on the relatively high radon concentrations (1550 ± 1080

200   mBq/m^3) and high average particle number counts (5721 ± 2680 cm^{-3}) [*Fitzgerald*, 1991;

201   *Hawkins et al.*, 2010; *O'Dowd and De Leeuw*, 2007; *Twohy et al.*, 2005]. Further evidence that

202   the Marine/Coastal Transport period is not entirely a clean marine period also stems from the

203   toluene to benzene ratio, which ranged from 0.030 during clean marine conditions to 3.74 when

204   fresh urban emissions were encountered with an average of 0.85.

205   3.1.4   Period 4: Ports of LA/LB

206   The Ports of LA/LB period was characterized by high $SO_{2(g)}$ concentrations (3.4 ± 5.2

207   ppbv on average with a maximum of 40 ppbv) compared to the previous periods when average

208     $SO_{2(g)}$ concentrations ranged from 0.06-0.45 ppbv. Further, low wind speeds (2.4 ± 1.2 m/s) and

209   low radon concentrations (740 ± 320 mBq/m^3) were also encountered. Toluene to benzene ratios

210   were high with an average of 1.89 and a maximum of 6.1 indicating a photo-chemically

211   unprocessed air mass. It is likely that local urban, port, and shipping emissions dominated the

212   particle composition during this period with little influence from other continental or transported

213   sources.

214   3.1.5   Period 5: Inland/Valley Transport

215   Figure 3e shows air masses traveling across the Central Valley and the desert before

216   traversing the LA Basin and Santa Barbara regions during the Inland/Valley Transport period.

217   Higher radon and $O_{3(g)}$ concentrations were measured during this time period compared to other

218   time periods with averages of 3200 ± 3000 mBq/m^3 and 44 ± 11 ppbv, respectively. Toluene to

219   benzene ratios had an average of 0.84 indicating that air masses sampled during this period were

220   fairly well-aged. Similar to Riverside, aerosol from the Central Valley is typically characterized

221   by high concentrations of secondary species, namely secondary organic aerosol and ammonium

222   nitrate due to contributions from dairy farms and other agricultural emissions in addition to urban

223   emissions from sources such as vehicles [*Chen et al.*, 2007; *Chow et al.*, 2006a; *Chow et al.*,

224   2006b; *Eatough et al.*, 2008]. Hence, particulate matter observed during this period is expected

225   to show similar signs of particle aging as the Riverside Transport period.

226   **3.1.6   Period 6: Bay Area/Sacramento**

227   During the Bay Area/Sacramento period, air masses traveled over the San Francisco Bay

228   area prior to arriving in the Sacramento region, which is within the Central Valley. Diurnal

229   temperature and RH profiles were observed with night and day values ranging from 16 to 30°C

230   and 24 to 93%, respectively. High toluene to benzene ratios were observed with an average of

231   1.74, suggesting that the sampled air masses were relatively fresh, similar to the Ports of LA/LB

232   period; however, unlike the Ports of LA/LB period, sampling during the Bay Area/Sacramento

233   period occurred within the Central Valley and not within a major port region.

234   **3.2   Observed Particle Types**

235   **3.2.1   Submicron Particle Composition**

236   Particle composition varied based on sources and transport conditions (Figures 2 and 4).

237   High number fractions of soot-containing particles (up to ~89% of submicron particles by

238   number with an average of ~38 ± 27%) were observed in Southern California, particularly during

239   the Riverside Transport, Stagnant/Ports Transport, and Ports of LA/LB periods (Periods 1, 2, and

240   4) when port and urban (e.g., vehicles) emissions were dominant. The main exception to this

241   trend in high soot-containing number fractions in Southern California occurred during the

242 Marine/Coastal Transport period (Period 3) when submicron particle composition was dominated

243 by sea salt particles (~63 ± 17% of submicron particles on average) due to air mass transport

244 conditions. The dominance of soot-containing particles in Southern California is in agreement

245 with aircraft ATOFMS measurements made during CalNex where *Cahill et al.*, [2012] reported

246 high soot-containing number fractions in the Southern California/LA Basin region.

247 In addition to the soot-containing particle type, particles from residual fuel combustion

248 (e.g., emissions from ships and oil refineries) were also observed namely during the

249 Stagnant/Ports Transport and Ports of LA/LB periods when port and shipping emissions heavily

250 influenced particle composition. This residual fuel combustion particle type represented at most

251 ~25% of submicron particles and is characterized by ion peaks associated with transition metals

252 found in residual fuel oil, notably vanadium ($^{51}V^+$, $^{67}VO^+$), nickel ($^{58,60}Ni^+$), and iron ($^{54,56}Fe^+$), in

253 addition to organic carbon, sulfate ($^{97}HSO_4^-$) and, to a lesser extent, nitrate ($^{46}NO_2^-$, $^{62}NO_3^-$) (see

254 Figure 5a for an example mass spectrum); these particles are herein referred to as V-OC particles

255 [*Agrawal et al.*, 2008; *Ault et al.*, 2010; *Ault et al.*, 2009; *Corbett and Fischbeck*, 1997; *Healy et*

256 *al.*, 2009; *Murphy et al.*, 2009]. During the Ports of LA/LB period, additional industrial particle

257 types were observed, including metals concentrated in the submicron size mode, which most

258 likely represent emissions from incineration [*Moffet et al.*, 2008a] and are the subject of a

259 different manuscript [*Weiss-Penzias et al.*, 2013]. Additionally, organic carbon (OC)

260 represented a much higher fraction of the detected submicron particles during the Ports of

261 LA/LB period (~14 ± 14% of the total submicron particles detected, on average) than previous

262 periods likely due to elevated fossil fuel emissions in the Ports of LA and LB from vehicles,

263 heavy duty diesel trucks and ships, which have been shown to contribute high mass

264 concentrations of organic carbon to the aerosol burden [*Lack et al.*, 2009; *Murphy et al.*, 2009;

265 *Russell et al.*, 2000; *Sodeman et al.*, 2005].

266   In contrast, soot-containing and V-OC particles made smaller contributions to the number

267 concentration in Southern California during Inland/Valley Transport conditions and in the

268 Northern California, Sacramento region during the Bay Area/Sacramento period (Periods 5-6).

269 As shown in Figures 2 and 4, particles from biomass burning were elevated in the submicron

270 mode during these two period representing up to ~61% of submicron particles. Biomass burning

271 particles are characterized by an intense potassium peak ($^{39}K^+$) in addition to carbonaceous peaks

272 (both elemental and organic), organic nitrogen peaks ($^{26}CN^-$, $^{42}CNO^-$), ion peaks associated with

273 potassium salts ($^{113}K_2Cl^+$, $^{213}K_3SO_4^+$, etc.), and secondary species such as sulfate and/or nitrate

274 (Figure 5b) [*Pratt et al.*, 2010; *Qin and Prather*, 2006; *Silva et al.*, 1999].

275   The key difference in particle composition observed in Northern California during the

276 Bay Area/Sacramento period (Period 6) was the high percentage of submicron OC particles

277 detected, constituting ~29 ± 23% of submicron particles by number on average and up to ~78%.

278 Unlike the OC detected during the Ports of LA/LB period, which originated from fossil fuel

279 sources in the Ports of LA and LB, OC detected in Sacramento is likely the result of biogenic

280 emissions due to the fact that biogenics were dominant during the first half of the Carbonaceous

281 Aerosol Radiative Effects Study (CARES) in the Sacramento Valley [*Cahill et al.*, 2012].

282 Numerous new particle formation (NPF) events were observed across the Sacramento Valley

283 during CalNex and the first part of CARES during this period [*Ahlm et al.*, 2012; *Setyan et al.*,

284 2012]. While the lower size limit of the nozzle-inlet ATOFMS (~0.2 um) cannot be used to

285 probe the composition of newly formed particles, ATOFMS measurements can provide insight

13

286   into the composition of these particles as they grow to sizes detectable by the instrument

287   [*Creamean et al.*, 2011]. Figure 6 shows particle number concentration as a function of diameter

288   measured by a differential mobility particle sizer (DMPS) [*Bates et al.*, 2012]. Two distinct

289   events are highlighted in black boxes when high number concentrations of small particles (~0.02

290   um) were observed followed by rapid growth, which is indicative of NPF events [*Creamean et*

291   *al.*, 2011; *Hegg and Baker*, 2009; *Kulmala*, 2003]. As shown in Figure 6, the percentage of OC

292   particles was smallest when the NPF event was actually occurring. This is because the size of

293   the newly formed particles is below the size detection limit of the instrument. The percentage of

294   OC particles increased primarily after these NPF events occurred as the newly formed particles

295   grew to sizes detectable by the instrument suggesting that organics contributed to this growth in

296   agreement with previous studies [*Creamean et al.*, 2011; *Kulmala*, 2003; *Smith et al.*, 2008;

297   *Zhang et al.*, 2004], and with recent measurements during CARES in the Sacramento Valley

298   from an aerosol mass spectrometer (AMS) [*Setyan et al.*, 2012]. The formation of new particles

299   occurred under conditions of lower RH and intense solar radiation; these low RH conditions also

300   favor the formation of high molecular weight secondary organic aerosol from biogenic emissions

301   that may have contributed to particle formation and/or growth [*Nguyen et al.*, 2011]. Growth of

302   these particles into sizes detectable by the ATOFMS occurred as RH increased with many of the

303   detected OC particles lacking negative ion spectra ($85 \pm 16\%$ on average) indicating that an

304   appreciable amount of particulate water was associated with these particles [*Neubauer et al.*,

305   1997; *Neubauer et al.*, 1998].

306   **3.2.2   Supermicron Particle Chemistry**

307   Aged sea salt dominated the supermicron particle composition during most periods

308   making up 50 ± 27% of total supermicron particles on average, as shown in Figures 2 and 4.

309   Aged sea salt particles result from heterogeneous reactions with gas-phase nitrogen oxides (e.g.,

310    $N_2O_{5(g)}$, $HNO_{3(g)}$), which lead to the displacement of chloride and the formation of particulate

311   nitrate [*Behnke et al.*, 1991; *Chang et al.*, 2011; *Gard et al.*, 1998; *Vogt et al.*, 1996]. In addition

312   to nitrate, methanesulfonic acid (MSA) and sulfate were also found on ~14% of aged sea salt

313   particles, on average, possibly contributing to the observed particulate chloride displacement

314   [*Hopkins et al.*, 2008; *Laskin et al.*, 2012]. During the Marine/Coastal Transport period (Period

315   3), fresh sea salt and marine biogenic particle types dominated the supermicron particle

316   composition making up 33 ± 11% and 30 ± 17% of supermicron particles on average,

317   respectively. Marine biogenic particle types include Mg-type [*Gaston et al.*, 2011] and sulfur-

318   type particles (C.J. Gaston et al., manuscript in preparation, 2013), which represent ocean-

319   derived particle types associated with marine biological activity and/or dissolved organic

320   material. The combined high wind speeds in addition to the elevated biological activity, as

321   evidenced by the presence of red tide blooms along the Southern California coast

322   (www.sccoos.org), explains the dominance of fresh sea salt and marine biogenic emissions

323   during this period.

324   Marine particle types were negligible in the inland, Sacramento region during the Bay

325   Area/Sacramento period. Instead, dust particles were found to represent 39 ± 23% of

326   supermicron particles, and biological particles were found to constitute up to ~64% of

327   supermicron particles as shown in Figures 2 and 4f. Most of the biological particles detected by

328   ATOFMS were determined to be spores containing dipicolinic acid, a compound that is easily

329   detected using laser/desorption ionization at 266 nm radiation and serves as a unique matrix

15

330   allowing for the detection of amino acids, which typically have low absorption cross sections at

331   266 nm [*Silva and Prather*, 2000; *Srivastava et al.*, 2005]. Consistent with previous

332   measurements of spores using laser/desorption ionization at 266 nm, spores detected during

333   CalNex contained $^{39}K^+$, $^{59}(CH_3)_3N^+$, $^{74}(CH_3)_4N^+$, *m/z* +86 due to either $(C_2H_5)_2NCH_2^+$ or the

334   amino acids [leucine-HCO_2] and [isoleucine–HCO_2], *m/z* +104, which is yet to be identified,

335   phosphate ($^{63}PO_2^-$, $^{79}PO_3^-$), organic nitrogen ($^{26}CN^-$, $^{42}CNO^-$), and *m/z* -123, which is most likely

336   due to dipicolinic acid-HCO_2 [*Srivastava et al.*, 2005] (Figure 5c). Spores have rarely been

337   detected by ATOFMS in ambient environments and represent a very unique particle type most

338   likely detected due to agricultural and biogenic emissions from the Sacramento area.

3.3   Variations in the Mixing-State of Carbonaceous Particle Types

3.3.1 Soot Particle Mixing-State

341   In addition to probing overall particle composition, observed differences in the mixing-

342   state of soot-dominated particles were also investigated (Figure 7a). These particles are

343   characterized by intense elemental carbon ion peaks ($^{12}C^+$, $^{36}C_3^+$, $^{48}C_4^+$,…C_n^+). A small

344   percentage of freshly emitted elemental carbon particles, herein referred to as "soot", contained

345   intense elemental carbon peaks indicative of long chain elemental carbon (e.g. elemental carbon

346   ion peaks extending out to higher masses in both the positive and negative ion spectra) with only

347   low intensity peaks from secondary species such as sulfate and/or nitrate [*Cahill et al.*, 2012;

348   *Moffet and Prather*, 2009]. Most of the soot-containing particles, however, contained intense

349   elemental carbon peaks that did not extend out to higher masses and were internally mixed with

350   low intensity organic peaks ($^{27}C_2H_3^+$, $^{43}C_2H_3O^+$, etc.) in addition to other secondary species (e.g.,

351   nitrate and/or sulfate) in agreement with aircraft observations during CalNex [*Cahill et al.*, 2012;

352 *Metcalf et al.*, 2012]. This second class of soot-containing particles is herein referred to as Aged

353 Soot particles, consistent with *Cahill et al.* [2012], and is further sub-divided into Aged Soot (No

354 Negatives), Aged Soot (Sulfate), Aged Soot (Nitrate), Aged Soot (Neg OC) particle classes.

355 Overall, the majority of Aged Soot particles (~62 ± 20% of soot-containing particles on average)

356 lacked negative ion spectra and are classified as Aged Soot (No Negatives) (see Figures 5d and

357 7a), with sizes peaking in number concentration at ~0.5-0.6 um and extending up into the

358 supermicron size range (Figure 4). The lack of negative ion spectra and larger sizes suggests that

359 these particles contained appreciable particulate water [*Moffet et al.*, 2008b; *Neubauer et al.*,

360 1997; *Neubauer et al.*, 1998] possibly due to cloud or fog processing.

361   The most striking trend shown in Figure 7a is the high percentage of Aged Soot (sulfate)

362 particles detected in Southern California (representing, on average, ~30 ± 18% of detected

363 submicron soot-containing particles during the Riverside Transport, Stagnant/Ports Transport,

364 Marine/Coastal Transport, Ports of LA/LB period) that decreased significantly to ~11 ± 10% as

365 the ship moved north along the California coast. Aged Soot (sulfate) particles are characterized

366 by intense sulfate peaks ($^{80}SO_3^-$, $^{97}HSO_4^-$) (Figure 5e) [*Moffet and Prather*, 2009]. This trend in

367 Aged Soot (sulfate) particles is in contrast to aircraft measurements made by ATOFMS, which

368 mainly observed internal mixtures of soot and nitrate as opposed to sulfate in Southern California

369 [*Cahill et al.*, 2012] due to the accumulation of ammonium nitrate coatings [*Metcalf et al.*, 2012].

370 The most likely explanation is that soot-containing particles were measured in the western port

371 regions of the LA Basin onboard the R/V Atlantis where fresh shipping and port emissions

372 prevailed as opposed to the more aged emissions sampled onboard the aircraft. Fresh emissions

373 from industrial sources at the port and ocean-going vessels contain high levels of $SO_{2(g)}$ leading

374 to elevated levels of particulate sulfate [*Agrawal et al.*, 2008; *Ault et al.*, 2010; *Corbett and*

17

375   *Fischbeck*, 1997; *Corbett and Koehler*, 2003].   During CalNex, Aged Soot (sulfate) particles

376   were typically found to peak at ~0.55 um on average, which is larger than expected for freshly

377   emitted soot particles [*Moffet and Prather*, 2009]; this is likely due to condensation and aqueous

378   phase processing of $SO_{2(g)}$, which has been shown to contribute high quantities of sulfate to

379   particles in this size range in the LA Basin [*Hegg*, 1985; *Hering and Friedlander*, 1982; *Meng*

380   *and Seinfeld*, 1994].   It should be noted that regulations were adopted in 2009 requiring ships to

381   switch from high sulfur to low sulfur fuel within 24 nautical miles of the California coast [*CARB*,

382   2009].   Hence, in addition to fresh port and shipping emissions, another potential source of

383   elevated sulfate on soot particles, particularly during Marine/Coastal Transport conditions

384   (Period 3), is the presence of red tide blooms in Southern Californian waters during CalNex

385   (www.sccoos.org) of *L. polyedrum*, a marine organism that has been shown to contribute

386   biogenic sulfur to aerosols [*Gaston et al.*, 2010].   Although ATOFMS cannot be used to

387   distinguish biogenic and anthropogenic sulfate, MSA, an ocean-derived biogenic form of sulfur,

388   can be detected and used to assess the possibility of biogenic contributions to detected sulfate

389   levels [*Gaston et al.*, 2010].   In fact, ~38% of Aged Soot (sulfate) particles, on average during

390   the Riverside, Stagnant/Ports, Marine, and Ports of LA/LB periods, were found to also contain

391   MSA with the highest percentage (~62% of Aged Soot (sulfate) particles) occurring during the

392   Marine/Coastal Transport period while the lowest percentage (~13% of Aged Soot (sulfate)

393   particles) was observed during the Ports of LA/LB period.   This suggests that at least some of the

394   observed sulfate was from a biogenic source.

395   Agricultural emissions were also found to impact soot mixing-state by contributing Aged

396   Soot (nitrate) particles, particularly during the Riverside Transport and Bay Area/Sacramento

397   periods and toward the end of the Stagnant/Ports Transport period, when air masses were

398   transported from the Central Valley. These particles had similar positive ion markers to the

399   Aged Soot (sulfate) particles, but contained nitrate peaks ($^{46}NO_2^-$, $^{62}NO_3^-$) that were more intense

400   than sulfate (see Figure 5f). This particle type has been shown to result from the acquisition of

401   nitrate namely formed through photo-chemically produced nitric acid ($HNO_{3(g)}$), which

402   condenses onto particles causing them to grow; aqueous phase processing may also contribute to

403   this growth and the acquisition of nitrate [*Moffet and Prather*, 2009; *Moffet et al.*, 2008b]. This

404   particle type represented up to ~33% of soot-containing particles and was observed to peak at a

405   larger size mode than the other soot-containing particle types at ~0.75 um during the campaign

406   (Figure 4).

407   In addition to Aged Soot (nitrate) particles, unique Aged Soot particles containing sulfate

408   and intense ions at *m/z* -43, -57, and -71 (see Figure 5g) were detected during a period of

409   agricultural influence (Inland/Valley Transport conditions). To the best of our knowledge,

410   mixtures of soot and these ions have never been detected before by ATOFMS. Since organic

411   peaks in Aged Soot particles typically appear as positive ions, this particle type has been labeled

412   Aged Soot (Neg OC). It is most likely that this particle type is derived from a unique, fresh

413   source near the sampling site, since these ion markers were not observed on other particle types.

414   Further evidence for this speculation comes from the fact that this particle type peaks at a smaller

415   size (~0.35 um) than the other soot-containing types, as shown in Figure 4e, suggesting a local

416   source. The unique organic markers likely correspond to $^{43}CH_3CO^-$, $^{57}C_2O_2H^-$, and $^{71}C_3H_3O_2^-$

417   [*McLafferty and Turecek*, 1993; *Silva et al.*, 1999; *Silva and Prather*, 2000] possibly due to

418   contributions from levoglucason and/or methylglyoxal (*m/z* -71), glyoxal (*m/z* -57), and

419   acetaldehyde (*m/z* -43) [*Silva et al.*, 1999; *Silva and Prather*, 2000]. These organic species could

420   represent secondary organic aerosol (SOA) formed from the photolytic processing of organics in

421   the aqueous phase [*Bateman et al.*, 2011]; this mechanism was suggested to contribute organic

422   components with elevated atomic O:C ratios during CalNex [*Duong et al.*, 2011]. Additional

423   field and laboratory measurements are required to confirm the identification of these ion peaks.

424   **3.3.2   The Mixing-State of Organic Particles**

425   In addition to soot-containing particles, the mixing-state of OC particles (e.g., non-soot

426   containing OC particles) was also investigated by examining temporal trends. These non-soot

427   containing OC particles are distinguished from the Aged Soot types described above in that these

428   particles are not characterized by intense elemental carbon peaks at *m/z* +12, +24, +36, etc., but

429   instead have *m/z* +27, +37, and/or +43 as the main positive ion peaks. Three types of OC

430   particles were identified during CalNex: OC (no negatives), OC (sulfate), and OC (nitrate).

431   Temporal trends of the OC particle types are shown in Figure 7b. Most OC particles were found

432   to lack negative ion spectra (~67 ± 37% on average) (see Figure 5h) and peaked in the 0.5-0.6

433   um size range (Figure 4) suggesting that they contained appreciable particulate water similar to

434   soot-containing particles. However, during Marine/Coastal and Inland/Valley Transport

435   conditions (Periods 3 and 5), OC particles containing intense sulfate peaks (see Figure 5i) were

436   more common, representing ~55 ± 40% of organic particles on average, likely due to photo-

437   chemically produced sulfate possibly derived from biogenic emissions. In addition to sulfate,

438   OC particles with intense nitrate peaks (see Figure 5j) were also observed namely at night during

439   the Marine/Coastal Transport, Ports of LA/LB, Inland/Valley Transport, and Bay

440   Area/Sacramento periods (Periods 3-6) and represented ~9 ± 17% of organic particles, on

441   average. Overall, OC (nitrate) particles peaked at a smaller particle size (~0.35 um) suggesting

442   that not all of the nitrate on these particles was due to photo-chemically-produced nitrate, which

443 typically leads to larger particle sizes. Instead, these observations suggest possible contributions

444 of organonitrates formed from reactions with gas-phase precursors and nitrate radical at night

445 that then condense onto particles [*Ng et al.*, 2008]; organonitrates were also found to contribute

446 to the organic aerosol burden during CalNex in Bakersfield, CA [*Rollins et al.*, 2012].

447   The OC types described above also frequently contained aromatic peaks ($^{51}C_4H_3^+$,

448 $^{63}C_5H_3^+$, $^{77}C_6H_5^+$, etc) [*Silva and Prather*, 2000], which have been associated with secondary

449 processing of organic species in vehicle exhaust [*Shields et al.*, 2007; *Sodeman et al.*, 2005;

450 *Spencer et al.*, 2006; *Toner et al.*, 2008] and humic substances formed from biomass burning

451 [*Holecek et al.*, 2007; *Mayol-Bracero et al.*, 2002; *Qin and Prather*, 2006]. OC particles also

452 contained ion peaks indicative of amines (e.g., $^{59}(CH_3)_3N^+$, $^{86}(C_2H_5)_2NCH_2^+$, $^{101}(C_2H_5)_3N^+$,

453 $^{118}(C_2H_5)_3NOH^+$, etc.), which are semi-volatile species that can partition onto pre-existing

454 particles [*Angelino et al.*, 2001; *Pratt et al.*, 2009; *Schade and Crutzen*, 1995], and oxidized

455 organic markers (e.g., $^{43}C_2H_3O^+$) that indicate the presence of SOA [*Qin et al.*, 2012] (see Figure

456 5h). Ternary plots were used to examine the prevalence of these compounds and to further

457 elucidate the mixing-state and sources of OC particles using the ion peaks $^{59}(CH_3)_3N^+$, $^{43}C_2H_3O^+$,

458 and $^{77}C_6H_5^+$ as markers for amines, SOA/oxidized organics, and aromatics, respectively (see

459 Figure 8).

460   Amines were found to dominate the OC mixing-state during the first two periods, with 65

461 ± 33% of OC particles containing intense amine markers during the Riverside Transport period

462 and 48 ± 44% during the Stagnant/Ports Transport period (Figure 8). Dairy farm emissions from

463 the Chino and Central Valley regions in addition to possible contributions from traffic emissions

464 wherein ammonia and amines can be produced from catalytic converters [*Fraser and Cass*,

465   1998; *Sodeman et al.*, 2005], explain the dominance of amines during these two time periods

466   [*Hughes et al.*, 2002; *Pastor et al.*, 2003; *Pratt et al.*, 2009; *Qin et al.*, 2012; *Schade and*

467   *Crutzen*, 1995; *Sorooshian et al.*, 2008].   Further, during these two periods, low temperatures

468   and the highest average RH values were measured on the ship; similar meteorological conditions

469   encountered during transport would also favor the detection of amines during these periods

470   [*Angelino et al.*, 2001].   Further, $18 \pm 23\%$ of OC particles contained intense amine markers

471   during the Ports of LA/LB period even though inland transport conditions were not encountered

472   suggesting that ports could contribute an industrial source of amines, possibly from vehicle

473   emissions including heavy duty diesel vehicles [*Bishop et al.*, 2012; *Fraser and Cass*, 1998;

474   *Sodeman et al.*, 2005].   Amines could also have resulted from marine biogenic emissions

475   [*Facchini et al.*, 2008a; *Sorooshian et al.*, 2009].

476   Oxidized organics were prevalent during Inland/Valley Transport conditions (Period 5)

477   (Figure 8e). The high O_3 concentrations and photo-chemically aged nature of the sampled air

478   masses suggest that the organics during the Inland/Valley Transport period resulted from

479   secondary rather than primary sources [*Na et al.*, 2004; *Qin et al.*, 2012]. Oxidized organics at

480   *m/z* +43 were also prevalent during the Stagnant/Ports Transport period, when photo-chemically

481   aged air masses were sampled, and dominant during Marine/Coastal Transport conditions

482   (Period 3), likely due to secondary contributions. Another source of the oxidized organics during

483   the Marine/Coastal Transport period could be organics from marine biogenic sources, such as

484   lipopolysaccharides, that have a higher oxygen content than organics from anthropogenic sources

485   [*Facchini et al.*, 2008b; *Ovadnevaite et al.*, 2011; *Russell et al.*, 2011; *Russell et al.*, 2010].

SOA from aromatics was more prevalent during the Ports of LA/LB and Bay Area/Sacramento periods than during any other periods; however, oxidized organics were still the most prevalent type of organic during these two periods. The increased frequency of aromatic markers in the Ports of LA and LB is likely due to increased emissions from diesel combustion by trucks [*Kasper et al.*, 2007; *Maricq*, 2007; *Shields et al.*, 2007; *Spencer et al.*, 2006] in addition to emissions from ships [*Kasper et al.*, 2007; *Lack et al.*, 2009; *Murphy et al.*, 2009; *Russell et al.*, 2009]. Oxidized organics and amines in Sacramento are likely from agricultural and biogenic emissions [*Chow et al.*, 2006b; *Setyan et al.*, 2012; *Sorooshian et al.*, 2008] while the observed SOA from aromatics are likely humic substances derived from biomass burning [*Holecek et al.*, 2007; *Mayol-Bracero et al.*, 2002].

4. Conclusions and Implications for California

Overall, we found that the chemical properties of aerosol particles differed widely across California based on particle source and transport conditions. As evidenced by the particle chemistry and mixing-state measured onboard the R/V Atlantis, Southern California was impacted by fresh shipping and vehicular emissions from cars and diesel trucks in addition to marine biogenic emissions. Soot-containing particles were the most prevalent submicron particles in Southern California and were typically mixed with sulfate while aromatic markers were found to contribute to organics due to residual fuel, distillate fuel, and gasoline combustion. These fresh emissions were episodically mixed with inland, agricultural emissions leading to the presence of secondary species such as amines. It is important to note that the particles measured in Southern California contained elevated levels of sulfate because these measurements focused on fresh emissions from the Ports of LA and LB; if these measurements were made further

508 inland of the ports, enhancements in nitrate namely due to particle aging and contributions of

509 ammonium nitrate, as seen by other measurements, would have been observed instead [*Cahill et*

510 *al.*, 2012; *Metcalf et al.*, 2012].

511   In contrast, Northern California was impacted by biogenic emissions from the forested

512 Sierra Nevada foothills and agricultural emissions as evidenced by the prevalence of organic

513 carbon [*Cahill et al.*, 2012; *Setyan et al.*, 2012]. Oxidized organic compounds were frequently

514 associated with particles during Inland/Valley transport conditions and in Sacramento, likely due

515 to contributions from SOA while aromatic markers observed in Sacramento are likely due to

516 contributions from biomass burning.

517   Overall, we found that the mixing-state of particles in California varies significantly on a

518 regional scale due to diverse local sources. Further, the mixing-state of particles from these local

519 emissions can be significantly altered based on differences in meteorological conditions and air

520 mass histories, which will most likely result in regional differences in the health, optical, and

521 cloud nucleating properties for the aerosol populations observed across California. This should

522 be taken into account when determining which emissions sources to regulate in order to mitigate

523 the adverse effects of aerosols on both human health and climate change.

References:

540

541 Agrawal, H., Q.G.J. Malloy, W.A. Welch, J.W. Miller, and D.R. Cocker (2008), In-use gaseous
542   and particulate matter emissions from a modern ocean going container vessel, *Atmos.*
543   *Environ.*, *42* (21), 5504-5510.
544 Ahlm, L., S. Liu, D.A. Day, L.M. Russell, R. Weber, D.R. Gentner, A.H. Goldstein, J.P.
545   DiGangi, S.B. Henry, F.N. Keutsch, T.C. VandenBoer, M.Z. Markovic, J.G. Murphy, X.
546   Ren, and S. Scheller (2012), Formation and growth of ultrafine particles from secondary
547   sources in Bakersfield, California, *J Geophys Res*, *117*, D00V08,
548   doi:10.1029/2011JD017144.
549 Allen, J.O. (2002), YAADA software toolkit to analyze single-particle mass spectral data:
550   Reference manual version 1.1, *Arizona State University*, http://www.yaada.org.
551 Angelino, S., D.T. Suess, and K.A. Prather (2001), Formation of aerosol particles from reactions
552   of secondary and tertiary alkylamines: Characterization by aerosol time-of-flight mass
553   spectrometry, *Environ. Sci. Tech.*, *35* (15), 3130-3138.
554 Ault, A.P., C.J. Gaston, Y. Wang, G. Dominguez, M.H. Thiemens, and K.A. Prather (2010),
555   Characterization of the single particle mixing state of individual ship plume events
556   measured at the Port of Los Angeles, *Environ. Sci. Tech.*, *44* (6), 1954-1961.
557 Ault, A.P., M.J. Moore, H. Furutani, and K.A. Prather (2009), Impact of emissions from the Los
558   Angeles port region on San Diego air quality during regional transport events, *Environ.*
559   *Sci. Tech.*, *43* (10), 3500-3506.
560 Bateman, A.P., S.A. Nizkorodov, J. Laskin, and A. Laskin (2011), Photolytic processing of
561   secondary organic aerosols dissolved in cloud droplets, *Phys. Chem. Chem. Phys.*, *13*,
562   12199-12212.
563 Bates, T.S., P.K. Quinn, D.J. Coffman, D.S. Covert, T.L. Miller, J.E. Johnson, G.R. Carmichael,
564   I. Uno, S.A. Guazzotti, D.A. Sodeman, K.A. Prather, M. Rivera, L.M. Russell, and J.T.
565   Merrill (2004), Marine boundary layer dust and pollutant transport associated with the
566   passage of a frontal system over eastern Asia, *J. Geophys. Res.-[Atmos.]*, *109* (D19S19),
567   doi:10.1029/2003JD004094.
568 Bates, T.S., P.K. Quinn, A.A. Frossard, L.M. Russell, J. Hakala, T. Petaja, M. Kulmala, D.S.
569   Covert, C.D. Cappa, S.-M. Li, K. Hayden, I. Nuaaman, R. McLaren, P. Massoli, M.R.
570   Canagaratna, T.B. Onasch, D. Sueper, D. Worsnop, and W.C. Keene (2012),
571   Measurements of ocean derived aerosol off the coast of California, *J Geophys Res*, *117*,
572   D00V15, doi:10.1029/2012JD017588.
573 Behnke, W., H.U. Kruger, V. Scheer, and C. Zetzsch (1991), Formation of Atomic Cl from Sea
574   Spray Via Photolysis of Nitryl Chloride - Determination of the Sticking Coefficient of
575   N_2O_5 on NaCl Aerosol, *J. Aerosol Sci.*, *22*, S609-S612.
576 Bishop, G.A., B.G. Schuchmann, and D.H. Stedman (2012), Emission changes resulting from the
577   San Pedro Bay, California ports truck retirement program, *Environ. Sci. Tech.*, *46*, 551-
578   558.
579 Blanchard, D.C., and A.H. Woodcock (1957), Bubble formation and modification in the sea and
580   its meteorological significance, *Tellus*, *9* (2), 145-158.
581 Bon, D.M., I.M. Ulbrich, J.A. de Gouw, C. Warneke, W.C. Kuster, M.L. Alexander, A. Baker,
582   A.J. Beyersdorf, D. Blake, R. Fall, J.L. Jimenez, S.C. Herndon, L.G. Huey, W.B.
583   Knighton, J. Ortega, S. Springston, and O. Vargas (2011), Measurements of volatile

organic compounds at a suburban ground site (T1) in Mexico City during the MILAGRO 2006 campaign: measurement comparison, emission ratios, and source attribution, *Atmos. Chem. Phys.*, *11*, 2399-2421.

Cahill, J.F., K. Suski, J. Seinfeld, R.A. Zaveri, and K.A. Prather (2012), The mixing state between northern and southern California measured during CARES and CalNEX 2010, *Atmos. Chem. Phys.*, *12*, 10989-11002, doi:10.5194/acp-12-10989-2012.

CARB, Final Regulation Order. Fuel Sulfur and Other Operational Requirements for Ocean-Going Vessels within California Waters and 24 Nautical Miles of the California Baseline, California Air Resources Board: Sacramento, CA, 2009.

Chang, W.L., P.V. Bhave, S.S. Brown, N. Riemer, J. Stutz, and D. Dabdub (2011), Heterogeneous atmospheric chemistry, ambient measurements, and model calculations of N_2O_5: A review, *Aerosol Sci. Tech.*, *45* (6), 665-695.

Chen, L.W.A., J.G. Watson, J.C. Chow, and K.L. Magliano (2007), Quantifying $PM_{2.5}$ source contributions for the San Joaquin Valley with multivariate receptor models, *Environ. Sci. Tech.*, *41* (8), 2818-2826.

Chow, J.C., L.W.A. Chen, J.G. Watson, D.H. Lowenthal, K.A. Magliano, K. Turkiewicz, and D.E. Lehrman (2006a), $PM_{2.5}$ chemical composition and spatiotemporal variability during the California Regional PM_{10}/$PM_{2.5}$ Air Quality Study (CRPAQS), *J. Geophys. Res.-[Atmos.]*, *111* (D10), D10S04, doi:10.1029/2005JD006457.

Chow, J.C., J.G. Watson, D.H. Lowenthal, L.W.A. Chen, and K.L. Magliano (2006b), Particulate carbon measurements in California's San Joaquin Valley, *Chemosphere*, *62* (3), 337-348.

Corbett, J.J., and P. Fischbeck (1997), Emissions from ships, *Science*, *278* (5339), 823-824.

Corbett, J.J., and H.W. Koehler (2003), Updated emissions from ocean shipping, *J. Geophys. Res.-[Atmos.]*, *108* (D20), 4650, doi:10.1029/2003JD003751.

Creamean, J.M., A.P. Ault, J.E. Ten Hoeve, M.Z. Jacobson, G.C. Roberts, and K.A. Prather (2011), Measurements of aerosol chemistry during new particle formation events at a remote rural mountain site, *Environ. Sci. Tech.*, *45* (19), 8208-8216.

Dall'Osto, M., R.M. Harrison, D.C.S. Beddows, E.J. Freney, M.R. Heal, and R.J. Donovan (2006), Single-particle detection efficiencies of aerosol time-of-flight mass spectrometry during the North Atlantic marine boundary layer experiment, *Environ. Sci. Tech.*, *40* (16), 5029-5035.

Docherty, K.S., E.A. Stone, I.M. Ulbrich, P.F. DeCarlo, D.C. Snyder, J.J. Schauer, R.E. Peltier, R.J. Weber, S.M. Murphy, J.H. Seinfeld, B.D. Grover, D.J. Eatough, and J.L. Jimenez (2008), Apportionment of primary and secondary organic aerosols in Southern California during the 2005 Study of Organic Aerosols in Riverside (SOAR-1), *Environ. Sci. Tech.*, *42* (20), 7655-7662.

Draxler, R.R., and G.D. Rolph (2011), HYSPLIT (HYbrid Single-Particle Lagrangian Integrated Trajectory) Model access via NOAA ARL READY Website (http://ready.arl.noaa.gov/HYSPLIT.php), *NOAA Air Resources Laboratory*, Silver Spring, MD.

Duong, H.T., A. Sorooshian, J.S. Craven, S.P. Hersey, A.R. Metcalf, X. Zhang, R.J. Weber, H.H. Jonsson, R.C. Flagan, and J.H. Seinfeld (2011), Water-soluble organic aerosol in the Los Angeles Basin and outflow regions: Airborne and ground measurements during the 2010 CalNex field campaign, *J. Geophys. Res.*, *116*, D00V04, doi:10.1029/2011JD016674.

Eatough, D.J., B.D. Grover, W.R. Woolwine, N.L. Eatough, R. Long, and R. Farber (2008), Source apportionment of 1 h semi-continuous data during the 2005 Study of Organic Aerosols in Riverside (SOAR) using positive matrix factorization, *Atmos. Environ.*, *42* (11), 2706-2719.

Facchini, M.C., S. Decesari, M. Rinaldi, C. Carbone, E. Finessi, M. Mircea, S. Fuzzi, F. Moretti, E. Tagliavini, D. Ceburnis, and C.D. O'Dowd (2008a), Important source of marine secondary organic aerosol from biogenic amines, *Environ. Sci. Tech.*, *42* (24), 9116-9121.

Facchini, M.C., M. Rinaldi, S. Decesari, C. Carbone, E. Finessi, M. Mircea, S. Fuzzi, D. Ceburnis, R. Flanagan, E.D. Nilsson, G. de Leeuw, M. Martino, J. Woeltjen, and C.D. O'Dowd (2008b), Primary submicron marine aerosol dominated by insoluble organic colloids and aggregates, *Geophys. Res. Lett.*, *35*, L17814, doi:10.1029/2008GL034210.

Fitzgerald, J.W. (1991), Marine aerosols: A review, *Atmos. Environ. A-Gen. Topics*, *25* (3-4), 533-545.

Fraser, M.P., and G.R. Cass (1998), Detection of excess ammonia emissions from in-use vehicles and the implications for fine particle control, *Environ. Sci. Tech.*, *32*, 1053-1057.

Gard, E., J.E. Mayer, B.D. Morrical, T. Dienes, D.P. Fergenson, and K.A. Prather (1997), Real-time analysis of individual atmospheric aerosol particles: Design and performance of a portable ATOFMS, *Anal. Chem.*, *69* (20), 4083-4091.

Gard, E.E., M.J. Kleeman, D.S. Gross, L.S. Hughes, J.O. Allen, B.D. Morrical, D.P. Fergenson, T. Dienes, M.E. Galli, R.J. Johnson, G.R. Cass, and K.A. Prather (1998), Direct observation of heterogeneous chemistry in the atmosphere, *Science*, *279* (5354), 1184-1187.

Gaston, C.J., H. Furutani, S.A. Guazzotti, K.R. Coffee, T.S. Bates, P.K. Quinn, L.I. Aluwihare, B.G. Mitchell, and K.A. Prather (2011), Unique ocean-derived particles serve as a proxy for changes in ocean chemistry, *J. Geophys. Res.-[Atmos.]*, *116*, D18310, doi:10.1029/2010JD015289.

Gaston, C.J., K.A. Pratt, X.Y. Qin, and K.A. Prather (2010), Real-time detection and mixing state of methanesulfonate in single particles at an inland urban location during a phytoplankton bloom, *Environ. Sci. Tech.*, *44* (5), 1566-1572.

Gelencser, A., K. Siszler, and J. Hlavay (1997), Toluene-benzene concentration ratio as a tool for characterizing the distance from vehicular emission sources, *Environ. Sci. Tech.*, *31*, 2869-2872.

Grover, B.D., N.L. Eatough, W.R. Woolwine, J.P. Cannon, D.J. Eatough, and R.W. Long (2008), Semi-continuous mass closure of the major components of fine particulate matter in Riverside, CA, *Atmos. Environ.*, *42*, 250-260.

Guazzotti, S.A., K.R. Coffee, and K.A. Prather (2001), Continuous measurements of size-resolved particle chemistry during INDOEX-Intensive Field Phase 99, *J. Geophys. Res.-[Atmos.]*, *106* (D22), 28607-28627.

Hawkins, L.N., L.M. Russell, D.S. Covert, P.K. Quinn, and T.S. Bates (2010), Carboxylic acids, sulfates, and organosulfates in processed continental organic aerosol over the southeast Pacific Ocean during VOCALS-REx 2008, *J. Geophys. Res.-[Atmos.]*, *115*, D13201, doi:10.1029/2009JD013276.

672 Healy, R.M., I.P. O'Connor, S. Hellebust, A. Allanic, J.R. Sodeau, and J.C. Wenger (2009),
673   Characterization of single particles from in-port ship emissions, *Atmos Environ*, *43*,
674   6408-6414.

675 Hegg, D.A. (1985), The importance of liquid-phase oxidation of SO_2 in the troposphere, *J.*
676   *Geophys. Res.*, *90* (D2), 3773-3779.

677 Hegg, D.A., and M.B. Baker (2009), Nucleation in the atmosphere, *Reports on Progress in*
678   *Physics*, *72* (5), doi:10.1088/0034-4885/72/5/056801.

679 Hering, S.V., and S.K. Friedlander (1982), Origins of aerosol sulfur size distributions in the Los
680   Angeles Basin, *Atmos Environ*, *16* (11), 2647-2656.

681 Holecek, J.C., M.T. Spencer, and K.A. Prather (2007), Analysis of rainwater samples:
682   Comparison of single particle residues with ambient particle chemistry from the northeast
683   Pacific and Indian oceans, *J. Geophys. Res.-[Atmos.]*, *112* (D22),
684   doi:10.1029/2006JD008269.

685 Hopkins, R.J., Y. Desyaterik, A.V. Tivanski, R.A. Zaveri, C.M. Berkowitz, T. Tyliszczak, M.K.
686   Gilles, and A. Laskin (2008), Chemical speciation of sulfur in marine cloud droplets and
687   particles: Analysis of individual particles from the marine boundary layer over the
688   California Current, *J. Geophys. Res.-[Atmos.]*, *113* (D4), D04209,
689   doi:10.1029/2007JD008954.

690 Hughes, L.S., J.O. Allen, P. Bhave, M.J. Kleeman, G.R. Cass, D.Y. Liu, D.F. Fergenson, B.D.
691   Morrical, and K.A. Prather (2000), Evolution of atmospheric particles along trajectories
692   crossing the Los Angeles basin, *Environ. Sci. Tech.*, *34* (15), 3058-3068.

693 Hughes, L.S., J.O. Allen, L.G. Salmon, P.R. Mayo, R.J. Johnson, and G.R. Cass (2002),
694   Evolution of nitrogen species air pollutants along trajectories crossing the Los Angeles
695   area, *Environ. Sci. Tech.*, *36* (18), 3928-3935.

696 Kasper, A., S. Aufdenblatten, A. Forss, M. Mohr, and H. Burtscher (2007), Particulate emissions
697   from a low-speed marine diesel engine, *Aerosol Sci. Tech.*, *41* (1), 24-32.

698 Kulmala, M. (2003), How particles nucleate and grow, *Science*, *302* (5647), 1000-1001.

699 Lack, D.A., J.J. Corbett, T. Onasch, B. Lerner, P. Massoli, P.K. Quinn, T.S. Bates, D.S. Covert,
700   D. Coffman, B. Sierau, S. Herndon, J. Allan, T. Baynard, E. Lovejoy, A.R. Ravishankara,
701   and E. Williams (2009), Particulate emissions from commercial shipping: Chemical,
702   physical, and optical properties, *J. Geophys. Res.-[Atmos.]*, *114*, D00F04,
703   doi:10.1029/2008JD011300.

704 Laskin, A., R.C. Moffet, M.K. Gilles, J.D. Fast, R.A. Zaveri, B. Wang, P. Nigge, and J.
705   Shutthanandan (2012), Tropospheric chemistry of internally mixed sea salt and organic
706   particles: Surprising reactivity of NaCl with weak organic acids, *J. Geophys. Res.*, *117*,
707   D15302, doi:10.1029/2012JD017743.

708 Liu, D.-Y., K.A. Prather, and S.V. Herring (2000), Variations in the size and chemical
709   composition of nitrate-containing particles in Riverside, CA, *Aerosol Sci. Tech.*, *33* (1-2),
710   71-86.

711 Magliano, K.L., V.M. Hughes, L.R. Chinkin, D.L. Coe, T.L. Haste, N. Kumar, and F.W.
712   Lurmann (1999), Spatial and temporal variations in PM_{10} and $PM_{2.5}$ source contributions
713   and comparison to emissions during the 1995 integrated monitoring study, *Atmos.*
714   *Environ.*, *33* (29), 4757-4773.

715 Maricq, M.M. (2007), Chemical characterization of particulate emissions from diesel engines: A
716   review, *J. Aerosol Sci.*, *38* (11), 1079-1118.

717   Mayol-Bracero, O.L., P. Guyon, B. Graham, G. Roberts, M.O. Andreae, S. Decesari, M.C.
718   Facchini, S. Fuzzi, and P. Artaxo (2002), Water-soluble organic compounds in biomass
719   burning aerosols over Amazonia - 2. Apportionment of the chemical composition and
720   importance of the polyacidic fraction, *J. Geophys. Res.-[Atmos.]*, *107* (D20), 8091,
721   doi:10.1029/2001JD000522.
722   McLafferty, F.W., and F. Turecek, *Interpretation of Mass Spetra*, University Science Books,
723   Sausalito, CA, 1993.
724   Meng, Z., and J.H. Seinfeld (1994), On the source of the submicrometer droplet mode of urban
725   and regional aerosols, *Aerosol Sci. Tech.*, *20*, 253-265.
726   Metcalf, A.R., J.S. Craven, J.J. Ensberg, J. Brioude, W. Angevine, A. Sorooshian, H.T. Duong,
727   H.H. Jonsson, R.C. Flagan, and J.H. Seinfeld (2012), Black carbon aerosol over the Los
728   Angeles Basin during CalNex, *J. Geophys. Res.*, *117*, D00V13,
729   doi:10.1029/2011JD017255.
730   Moffet, R.C., Y. Desyaterik, R.J. Hopkins, A.V. Tivanski, M.K. Gilles, Y. Wang, V.
731   Shutthanandan, L.T. Molina, R.G. Abraham, K.S. Johnson, V. Mugica, M.J. Molina, A.
732   Laskin, and K.A. Prather (2008a), Characterization of aerosols containing Zn, Pb, and Cl
733   from an industrial region of Mexico City, *Environ. Sci. Tech.*, *42* (19), 7091-7097.
734   Moffet, R.C., and K.A. Prather (2009), In-situ measurements of the mixing state and optical
735   properties of soot with implications for radiative forcing estimates, *PNAS*, *106* (29),
736   11872-11877.
737   Moffet, R.C., X. Qin, T. Rebotier, H. Furutani, and K.A. Prather (2008b), Chemically segregated
738   optical and microphysical properties of ambient aerosols measured in a single-particle
739   mass spectrometer, *J. Geophys. Res.*, *113* (D12213), D12213,
740   doi:10.1029/2007JD009393.
741   Monahan, E.C., C.W. Fairall, K.L. Davidson, and P.J. Boyle (1983), Observed interrelations
742   between 10m winds, ocean whitecaps and marine aerosols, *Quarterly Journal of the*
743   *Royal Meteorological Society*, *109* (460), 379-392.
744   Murphy, S.M.A., H.; Sorooshian, A.; Padro, L. T.; Gates, S.W. H.; Hersey, W. A.; Jung, H.;
745   Miller, J. W.; Cocker, D. R., and A.J. Nenes, H. H.; Flagan, R. C.; Seinfeld, J. H. (2009),
746   Comprehensive simultaneous shipboard and airborne characterization of exhaust from a
747   modern container ship at sea., *Environ. Sci. Tech.*, *43* (13), 4626-4640.
748   Na, K., A.A. Sawant, C. Song, and D.R. Cocker (2004), Primary and secondary carbonaceous
749   species in the atmosphere of Western Riverside County, California, *Atmos Environ*, *38*,
750   1345-1355.
751   Neubauer, K.R., M.V. Johnston, and A.S. Wexler (1997), On-line analysis of aqueous aerosols
752   by laser desorption ionization, *International Journal of Mass Spectrometry and Ion*
753   *Processes*, *163* (1-2), 29-37.
754   Neubauer, K.R., M.V. Johnston, and A.S. Wexler (1998), Humidity effects on the mass spectra
755   of single aerosol particles, *Atmos. Environ.*, *32* (14-15), 2521-2529.
756   Ng, N.L., A.J. Kwan, J.D. Surratt, A.W.H. Chan, P.S. Chhabra, A. Sorooshian, H.O.T. Pye, J.D.
757   Crounse, P.O. Wennberg, R.C. Flagan, and J.H. Seinfeld (2008), Secondary organic
758   aerosol (SOA) formation from reaction of isoprene with nitrate radicals (NO_3), *Atmos.*
759   *Chem. Phys.*, *8* (14), 4117-4140.

Nguyen, T.B., P.J. Roach, J. Laskin, A. Laskin, and S.A. Nizkorodov (2011), Effect of humidity on the composition of isoprene photooxidation secondary organic aerosol, *Atmos. Chem. Phys.*, *11*, 6931-6944.

Noble, C.A., and K.A. Prather (1996), Real-time measurement of correlated size and composition profiles of individual atmospheric aerosol particles, *Environ. Sci. Tech.*, *30* (9), 2667-2680.

O'Dowd, C.D., and G. De Leeuw (2007), Marine aerosol production: a review of the current knowledge, *Phil. Trans. A*, *365* (1856), 1753-1774.

Ovadnevaite, J., C. O'Dowd, M. Dall'Osto, D. Ceburnis, D.R. Worsnop, and H. Berresheim (2011), Detecting high contributions of primary organic matter to marine aerosol: A case study, *Geophys. Res. Lett.*, *38*, L02807, doi:10.1029/2010GL046083.

Pastor, S.H., J.O. Allen, L.S. Hughes, P. Bhave, G.R. Cass, and K.A. Prather (2003), Ambient single particle analysis in Riverside, California by aerosol time-of-flight mass spectrometry during the SCOS97-NARSTO, *Atmos. Environ.*, *37*, S239-S258.

Poschl, U. (2005), Atmospheric aerosols: Composition, transformation, climate and health effects, *Angewandte Chemie-International Edition*, *44* (46), 7520-7540.

Prather, K.A., T. Nordmeyer, and K. Salt (1994), Real-Time Characterization of Individual Aerosol-Particles Using Time-of-Flight Mass-Spectrometry, *Anal. Chem.*, *66* (9), 1403-1407.

Pratt, K.A., L.E. Hatch, and K.A. Prather (2009), Seasonal volatility dependence of ambient particle phase amines, *Environ. Sci. Tech.*, *43* (14), 5276-5281.

Pratt, K.A., A.J. Heymsfield, C.H. Twohy, S.M. Murphy, P.J. DeMott, J.G. Hudson, R. Subramanian, Z.E. Wang, J.H. Seinfeld, and K.A. Prather (2010), In Situ Chemical Characterization of Aged Biomass-Burning Aerosols Impacting Cold Wave Clouds, *J. Atmos. Sci.*, *67* (8), 2451-2468.

Pratt, K.A., and K.A. Prather (2009), Real-time, single-particle volatility, size, and chemical composition measurements of aged urban aerosols, *Environ. Sci. Tech.*, *43* (21), 8276-8282.

Pratt, K.A., and K.A. Prather (2011), Mass spectrometry of atmospheric aerosols—Recent developments and applications. Part II: On-line mass spectrometry techniques, *Mass Spectrometry Reviews*, DOI 10.1002/mas.20330.

Qin, X., K.A. Pratt, L.G. Shields, S.M. Toner, and K.A. Prather (2012), Seasonal comparisons of single-particle chemical mixing state in Riverside, CA, *Atmos. Environ.*, *59*, 587-596.

Qin, X.Y., P.V. Bhave, and K.A. Prather (2006), Comparison of two methods for obtaining quantitative mass concentrations from aerosol time-of-flight mass spectrometry measurements, *Anal. Chem.*, *78* (17), 6169-6178.

Qin, X.Y., and K.A. Prather (2006), Impact of biomass emissions on particle chemistry during the California Regional Particulate Air Quality Study, *International Journal of Mass Spectrometry*, *258* (1-3), 142-150.

Quinn, P.K., and T.S. Bates (2005), Regional aerosol properties: Comparisons of boundary layer measurements from ACE 1, ACE 2, Aerosols99, INDOEX, ACE Asia, TARFOX, and NEAQS, *J. Geophys. Res.*, *110* (D14202), doi:10.1029/2004JD004755.

Roberts, J.M., F.C. Fehsenfeld, S.C. Liu, M.J. Bollinger, C. Hahn, D.L. Albritton, and R.E. Sievers (1984), Measurements of aromatic hydrocarbon ratios and NO_x concentrations in

the rural troposphere: Observation of air mass photochemical aging and NO$_x$ removal, *Atmos Environ*, *18* (11), 2421-2432.

Rollins, A.W., E.C. Browne, K.-E. Min, S.E. Pusede, P.J. Wooldridge, D.R. Gentner, A.H. Goldstein, S. Liu, D.A. Day, L.M. Russell, and R.C. Cohen (2012), Evidence for NO$_x$ control over nighttime SOA formation, *Science*, *337* (6099), 1210-1212.

Russell, L.M., R. Bahadur, and P.J. Ziemann (2011), Identifying organic aerosol sources by comparing functional group composition in chamber and atmospheric particles, *PNAS*, doi:10.1073/pnas.1006461108.

Russell, L.M., L.N. Hawkins, A.A. Frossard, P.K. Quinn, and T.S. Bates (2010), Carbohydrate-like composition of submicron atmospheric particles and their production from ocean bubble bursting, *PNAS*, *107* (15), 6652-6657.

Russell, L.M., K.J. Noone, R.J. Ferek, R.A. Pockalny, R.C. Flagan, and J.H. Seinfeld (2000), Combustion organic aerosol as cloud condensation nuclei in ship tracks, *American Meteorological Society*, 2591-2606.

Russell, L.M., S. Takahama, S. Liu, L.N. Hawkins, D.S. Covert, P.K. Quinn, and T.S. Bates (2009), Oxygenated fraction and mass of organic aerosol from direct emission and atmospheric processing measured on the R/V Ronald Brown during TEXAQS/GoMACCS 2006, *J. Geophys. Res.-[Atmos.]*, *114*, D00F05, doi:10.1029/2008JD011275.

Ryerson, T.B., A.E. Andrews, W.M. Angevine, T.S. Bates, C.A. Brock, B. Cairns, R.C. Cohen, O.R. Cooper, J.A. de Gouw, F.C. Fehsenfeld, R.A. Ferrare, M.L. Fischer, R.C. Flagan, A.H. Goldstein, J.W. Hair, R.M. Hardesty, C.A. Hostetler, J.L. Jimenez, A.O. Langford, E. McCauley, S.A. McKeen, L.T. Molina, A. Nenes, S.J. Oltmans, D.D. Parrish, J.R. Pederson, R.B. Pierce, K.A. Prather, P.K. Quinn, J.H. Seinfeld, C.J. Senff, A. Sorooshian, J. Stutz, J.D. Surratt, M. Trainer, R. Volkamer, E.J. Williams, and S.C. Wofsy (2013), The 2010 California Research at the Nexus of Air Quality and Climate Change (CalNex) field study, *J. Geophys. Res.*, In Press.

Schade, G.W., and P.J. Crutzen (1995), Emission of aliphatic amines from animal husbandry and their reactions: Potential source of N$_2$O and HCN, *J. Atmos. Chem.*, *22* (3), 319-346.

Setyan, A., Q. Zhang, M. Merkel, W.B. Knighton, Y. Sun, C. Song, J.E. Shilling, T.B. Onasch, S.C. Herndon, D. Worsnop, J.D. Fast, R.A. Zaveri, L.K. Berg, A. Wiedensohler, B.A. Flowers, M.K. Dubey, and R. Subramanian (2012), Characterization of submicron particles influenced by mixed biogenic and anthropogenic using high-resolution aerosol mass spectrometry: Results from CARES, *Atmos. Chem. Phys.*, *12*, 8131-8156.

Shields, L.G., D.T. Suess, and K.A. Prather (2007), Determination of single particle mass spectral signatures from heavy-duty diesel vehicle emissions for PM$_{2.5}$ source apportionment, *Atmos. Environ.*, *41* (18), 3841-3852.

Silva, P.J., D.Y. Liu, C.A. Noble, and K.A. Prather (1999), Size and chemical characterization of individual particles resulting from biomass burning of local Southern California species, *Environ. Sci. Tech.*, *33* (18), 3068-3076.

Silva, P.J., and K.A. Prather (2000), Interpretation of mass spectra from organic compounds in aerosol time-of-flight mass spectrometry, *Anal. Chem.*, *72* (15), 3553-3562.

Smith, J.N., M.J. Dunn, T.M. VanReken, K. Iida, M.R. Stolzenburg, P.H. McMurry, and L.G. Huey (2008), Chemical composition of atmospheric nanoparticles formed from

nucleation in Tecamac, Mexico: Evidence for an important role for organic species in nanoparticle growth, *Geophys. Res. Lett.*, *35* (4), L04808, doi:10.1029/2007GL032523.

Sodeman, D.A., S.M. Toner, and K.A. Prather (2005), Determination of single particle mass spectral signatures from light-duty vehicle emissions, *Environ. Sci. Tech.*, *39* (12), 4569-4580.

Song, X.H., P.K. Hopke, D.P. Fergenson, and K.A. Prather (1999), Classification of single particles analyzed by ATOFMS using an artificial neural network, ART-2a, *Anal. Chem.*, *71* (4), 860-865.

Sorooshian, A., S.N. Murphy, S. Hersey, H. Gates, L.T. Padro, A. Nenes, F.J. Brechtel, H. Jonsson, R.C. Flagan, and J.H. Seinfeld (2008), Comprehensive airborne characterization of aerosol from a major bovine source, *Atmos. Chem. Phys.*, *8* (17), 5489-5520.

Sorooshian, A., L.T. Padro, A. Nenes, G. Feingold, A. McComiskey, S.P. Hersey, H. Gates, H.H. Jonsson, S.D. Miller, G.L. Stephens, R.C. Flagan, and J.H. Seinfeld (2009), On the link between ocean biota emissions, aerosol, and maritime clouds: Airborne, ground, and satellite measurements off the coast of California, *Glob. Biogeochem. Cy.*, *23*, GB4007, doi:10.1029/2009GB003464.

Spencer, M.T., L.G. Shields, D.A. Sodeman, S.M. Toner, and K.A. Prather (2006), Comparison of oil and fuel particle chemical signatures with particle emissions from heavy and light duty vehicles, *Atmos. Environ.*, *40* (27), 5224-5235.

Srivastava, A., M.E. Pitesky, P.T. Steele, H.J. Tobias, D.P. Fergenson, J.M. Horn, S.C. Russell, G.A. Czerwieniec, C.S. Lebrilla, E.E. Gard, and M. Frank (2005), Comprehensive assignment of mass spectral signatures from individual Bacillus atrophaeus spores in matrix-free laser desorption/ionization bioaerosol mass spectrometry, *Anal. Chem.*, *77* (10), 3315-3323.

Sullivan, R.C., and K.A. Prather (2005), Recent advances in our understanding of atmospheric chemistry and climate made possible by on-line aerosol analysis instrumentation, *Anal. Chem.*, *77* (12), 3861-3885.

Toner, S.M., L.G. Shields, D.A. Sodeman, and K.A. Prather (2008), Using mass spectral source signatures to apportion exhaust particles from gasoline and diesel powered vehicles in a freeway study using UF-ATOFMS, *Atmos. Environ.*, *42* (3), 568-581.

Twohy, C.H., M.D. Petters, J.R. Snider, B. Stevens, W. Tahnk, M. Wetzel, L. Russell, and F. Burnet (2005), Evaluation of the aerosol indirect effect in marine stratocumulus clouds: Droplet number, size, liquid water path, and radiative impact, *J. Geophys. Res.-[Atmos.]*, *110* (D8), doi:10.1029/2004JD005116.

Vogt, R., P.J. Crutzen, and R. Sander (1996), A mechanism for halogen release from sea-salt aerosol in the remote marine boundary layer, *Nature*, *383* (6598), 327-330.

Weiss-Penzias, P., E. Williams, B. Lerner, T. Bates, C. Gaston, K. Prather, A. Vlasenko, and S.-M. Li (2013), Shipboard Measurements of Gaseous Elemental Mercury along the Coast of Central and Southern California, *Journal of Geophysical Research-[Atmos]*, *118*, DOI: 10.1029/2012JD018463.

Wenzel, R.J., D.Y. Liu, E.S. Edgerton, and K.A. Prather (2003), Aerosol time-of-flight mass spectrometry during the Atlanta Supersite Experiment: 2. Scaling procedures, *J. Geophys. Res.-[Atmos.]*, *108* (D7), 8427,doi:10.1029/2001JD001563.

891   Whiteaker, J.R., D.T. Suess, and K.A. Prather (2002), Effects of meteorological conditions on
892   aerosol composition and mixing state in Bakersfield, CA, *Environ. Sci. Tech.*, *36* (11),
893   2345-2353.
894   Zhang, Q., C.O. Stanier, M.R. Canagaratna, J.T. Jayne, D.R. Worsnop, S.N. Pandis, and J.L.
895   Jimenez (2004), Insights into the chemistry of new particle formation and growth events
896   in Pittsburgh based on aerosol mass spectrometry, *Environ. Sci. Tech.*, *38* (18), 4797-
897   4809.
898
899

900 **Table 1:** Meteorological and Gas Phase Data for 6 Different Air Mass Transport
901 Conditions. Day of Year (DOY), date and time (UTC), latitudinal and longitudinal range,
902 average meteorological conditions (wind speed, RH, air temperature), and average gas-phase
903 concentrations (radon, SO_2, ozone, and the toluene/benzene ratio) for measurements made during
904 each of the 6 different time periods are highlighted.

905

Period	Location/ Air Mass	Day of Year (DOY)	Date and Time (UTC)	Latitude	Longitude	Wind Speed (m/s)	RH (%)	Air Temp (°C)	Radon (mBq/m^3)	SO$_2$ (ppbv)	Ozone (ppbv)	Toluene/ Benzene
1	Riverside	135.5-137.375	5/15/2010 12:00-5/17/2010 9:00	33.14N to 34.02N	118.33W to 119.22W	2.93	89	13.2	2500	0.07	47.1	N/A
2	Stagnant/ Ports	137.375-140.5	5/17/2010 9:00-5/20/2010 12:00	33.67N to 34.38N	118.22W to 119.69W	3.86	91	13.4	1060	0.06	39.0	0.40
3	Marine/ Coastal	142-146	5/22/2010 0:00-5/26/2010 0:00	33.31N to 33.95N	118.07W to 118.93W	5.18	72	13.9	1550	0.14	35.1	0.85
4	Ports of LA/LB	146.33-147.875	5/26/2010 8:00-5/27/2010 21:00	33.53N to 33.77N	118.1W to 118.5W	2.40	73	16.0	740	3.40	29.3	1.89
5	Inland/ Valley	149-151.875	5/29/2010 0:00-5/31/2010 21:00	33.5N to 34.4N	118.17W to 119.85W	3.29	83	15.2	3200	0.45	43.6	0.84
6	Bay Area/ Sacramento	154.625-157.625	6/3/2010 15:00-6/6/2010 15:00	38.02N to 38.56N	121.55 W to 122.16W	4.53	69	20.9	1550	0.42	22.8	1.74

907

908

909
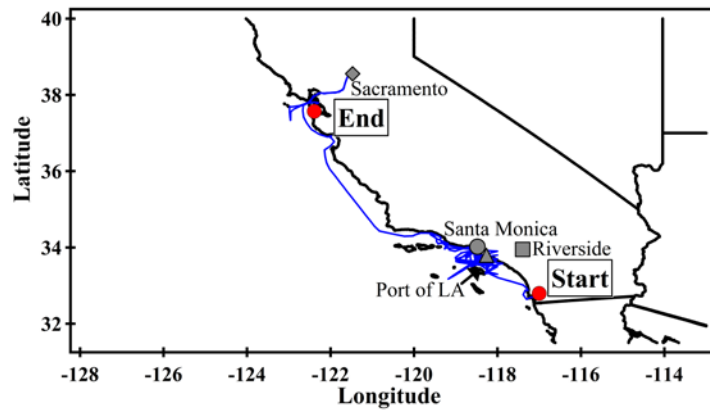
910
911 **Figure 1:** Cruise track for the R/V Atlantis (blue line) along the California coast during CalNex.

912 The Port of Los Angeles (grey triangle), the Santa Monica area (grey dot), Riverside (grey

913 square) and the Sacramento area (grey diamond) are shown along with the start and end points of
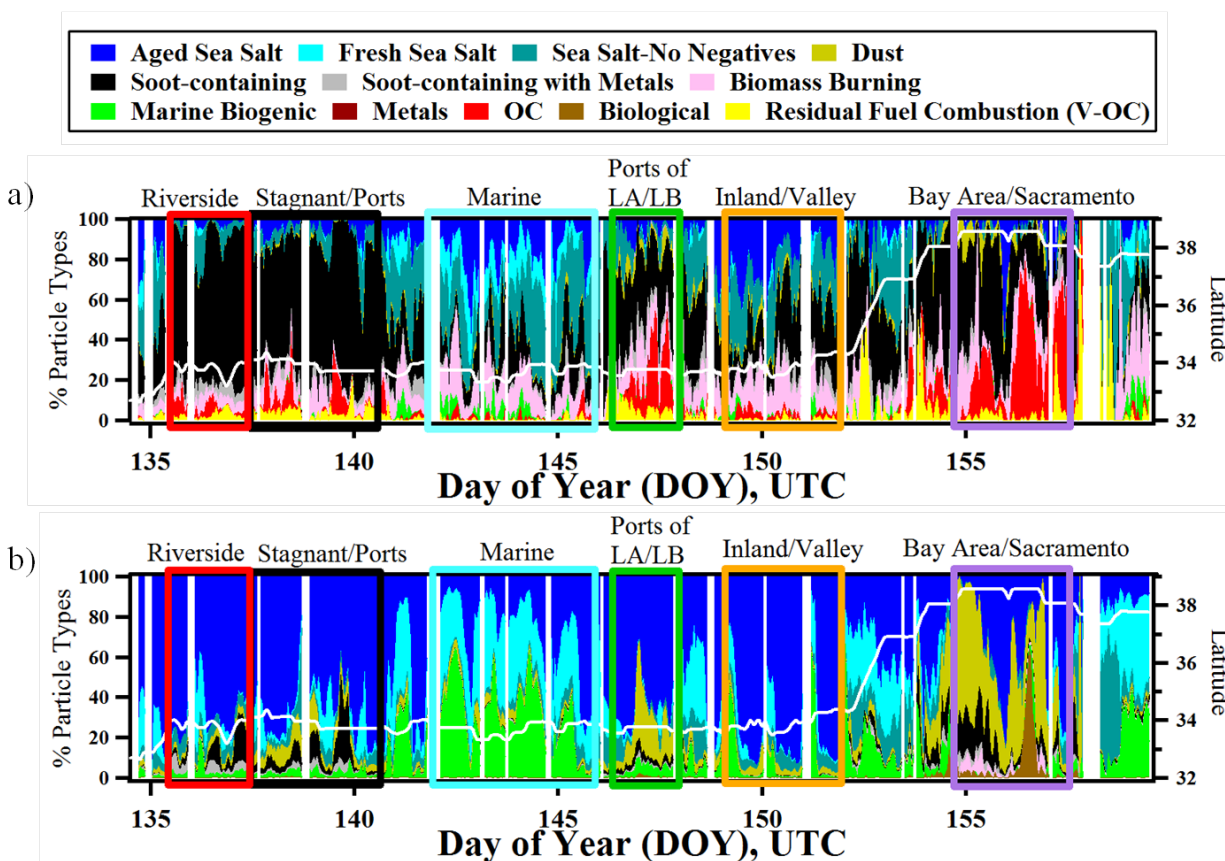
914 the cruise.

915
916
917
918

Figure 2: Hourly temporal profile of single-particle mixing-state observed by ATOFMS in UTC

as a function of day of year (DOY) and latitude (white line). The (a) top and (b) bottom panels

show the single-particle chemistry for submicron particles (0.2-1.0 μm) and supermicron

particles (1.0-3.0 μm), respectively. Colored boxes highlight 6 different periods when

differences in particle composition were observed due to different meteorological conditions,

gas-phase concentrations, and aging processes.
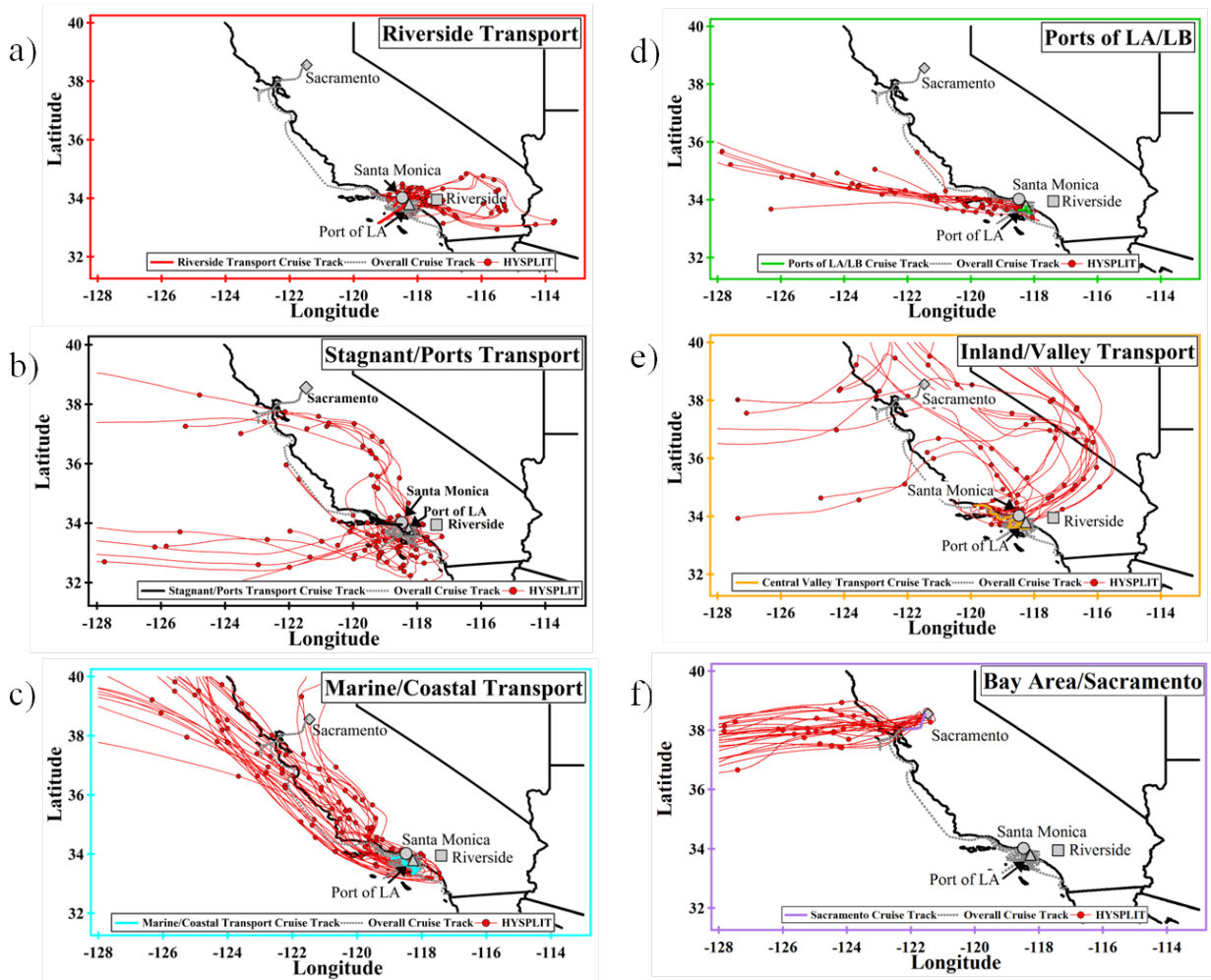
Figure 3: 48-hour HYSPLIT air mass back-trajectories at 500 m (red lines) shown during the cruise (grey dotted line) corresponding to (a) Period 1: Riverside Transport boxed in red, (b) Period 2: Stagnant/Ports Transport boxed in black, (c) Period 3: Marine/Coastal Transport boxed in cyan, (d) Period 4: Ports of LA/LB boxed in green, (e) Period 5: Inland/Valley Transport boxed in orange, and (f) Period 6: Bay Area/Sacramento boxed in purple. Red dots on the HYSPLIT trajectories denote 12 hour increments. The Port of Los Angeles (grey triangle), the Santa Monica area (grey dot), Riverside (grey square) and the Sacramento area (grey diamond) are also shown.
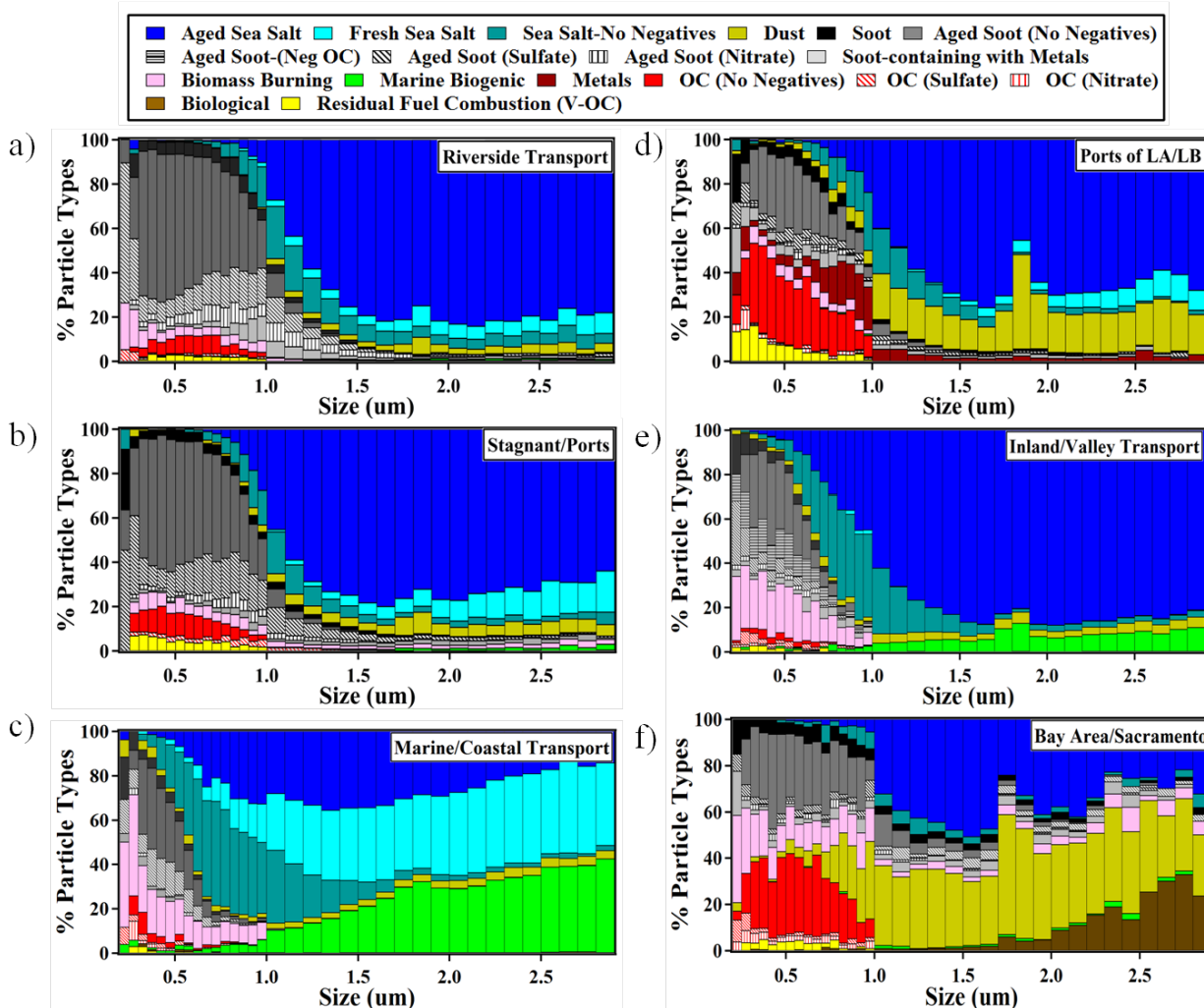
Figure 4: Fraction of particle types as a function of size observed during the 6 different time periods. Submicron particles (0.2-1.0 μm) are plotted in 0.05 μm bins while supermicron particles (1.0-3.0 μm) are plotted in 0.1 μm bins.
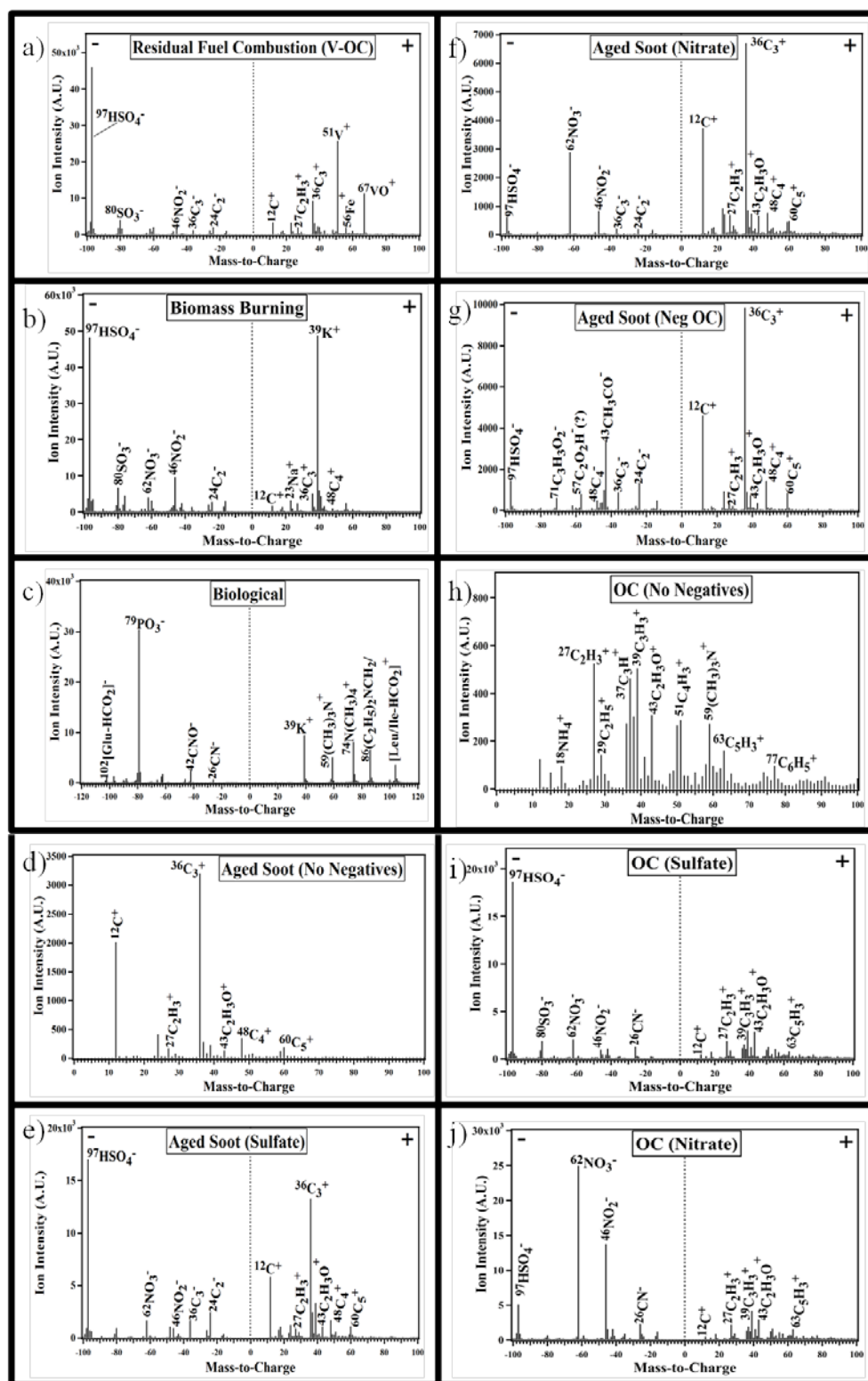
942

943

944 **Figure 5:** Representative mass spectra of (a) Residual Fuel Combustion from ships (V-OC), (b)

945 Biomass Burning, (c) Biological, (d) Aged Soot (No Negatives), (e) Aged Soot (Sulfate), (f)

946 Aged Soot (Nitrate), (g) Aged Soot (Neg OC), (h) OC (No Negatives), (i) OC (Sulfate), (j) OC

947 (Nitrate) particles are shown. For mass spectra containing both positive and negative ions,

948 dashed lines separate negative ions (left side) and positive ions (right side).

949

950
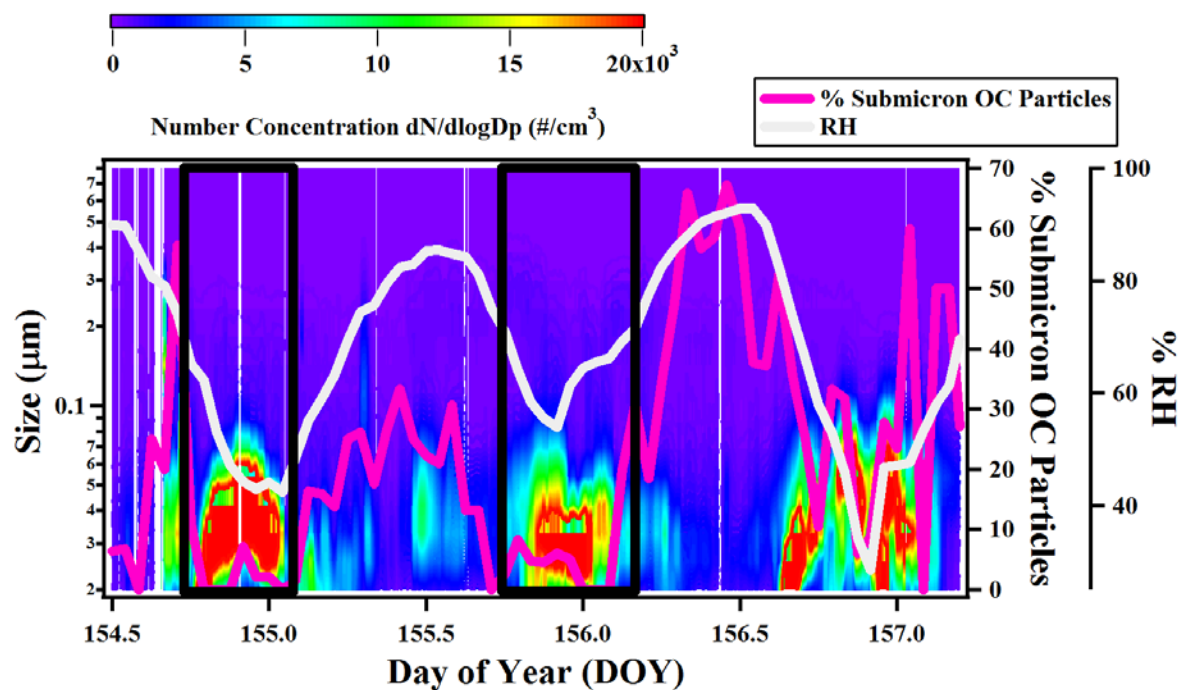
951
952 **Figure 6:** Size distributions of particle number concentrations as a function of size and DOY

953 are shown on a log scale. The percentage of submicron OC particles detected by ATOFMS

954 (pink line) and RH (grey line) are shown as a function of DOY. Time periods when new particle

955 formation events were observed are shown in black boxes.
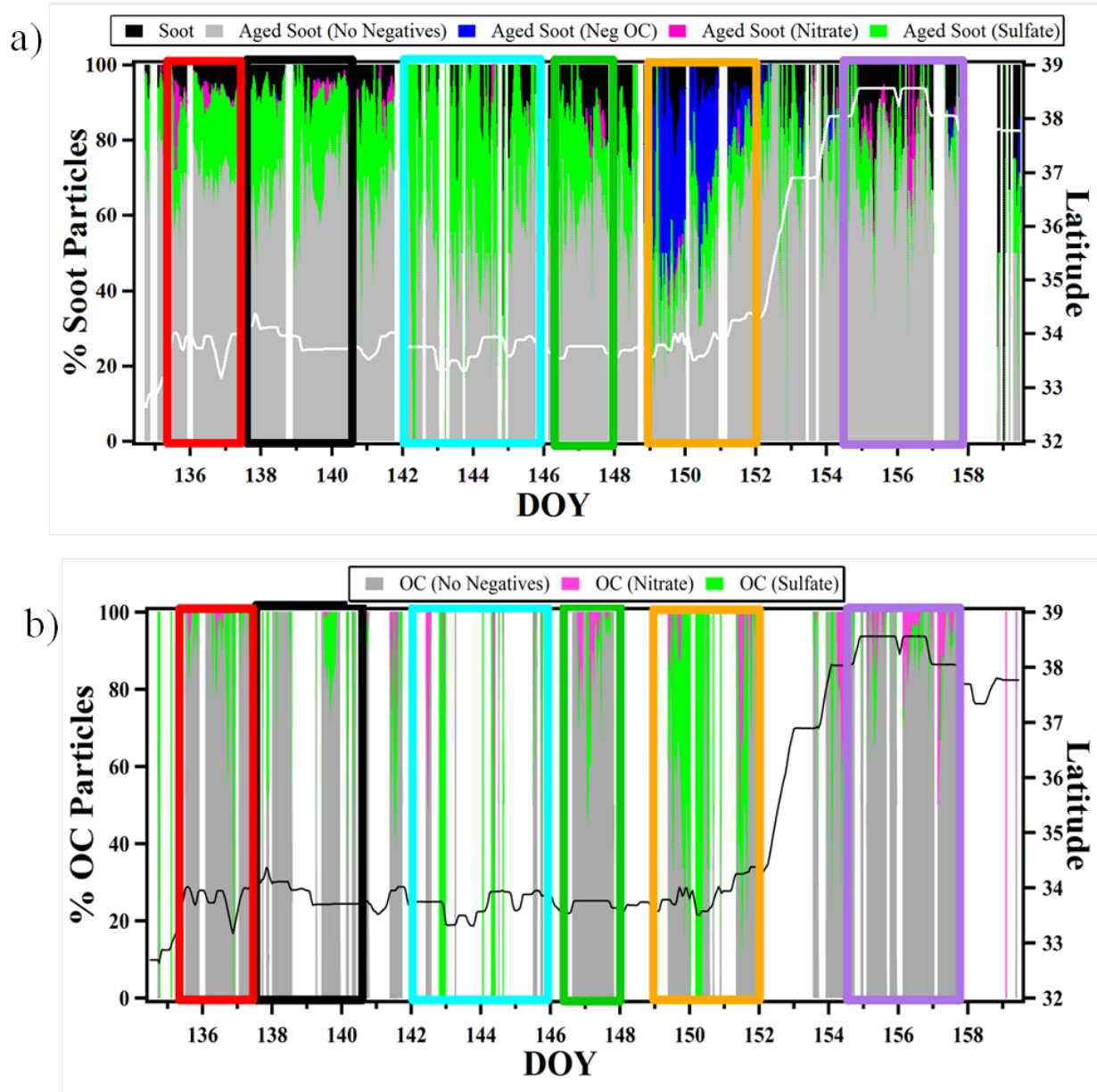
956
957

43

Figure 7: Hourly temporal trends in carbonaceous mixing-state. The top panel (a) shows hourly temporal trends for different soot particle types: Soot (black), Aged Soot (No Negatives) (grey), Aged Soot (Sulfate) (green), Aged Soot (Nitrate) (pink), and Aged Soot (Neg OC) (blue) in addition to latitude (white line). The bottom panel (b) shows hourly temporal trends for different organic particle types: OC (No Negatives) (grey), OC (Sulfate) (green), and OC (Nitrate) (pink) in addition to latitude (black line). The 6 different time periods are boxed.
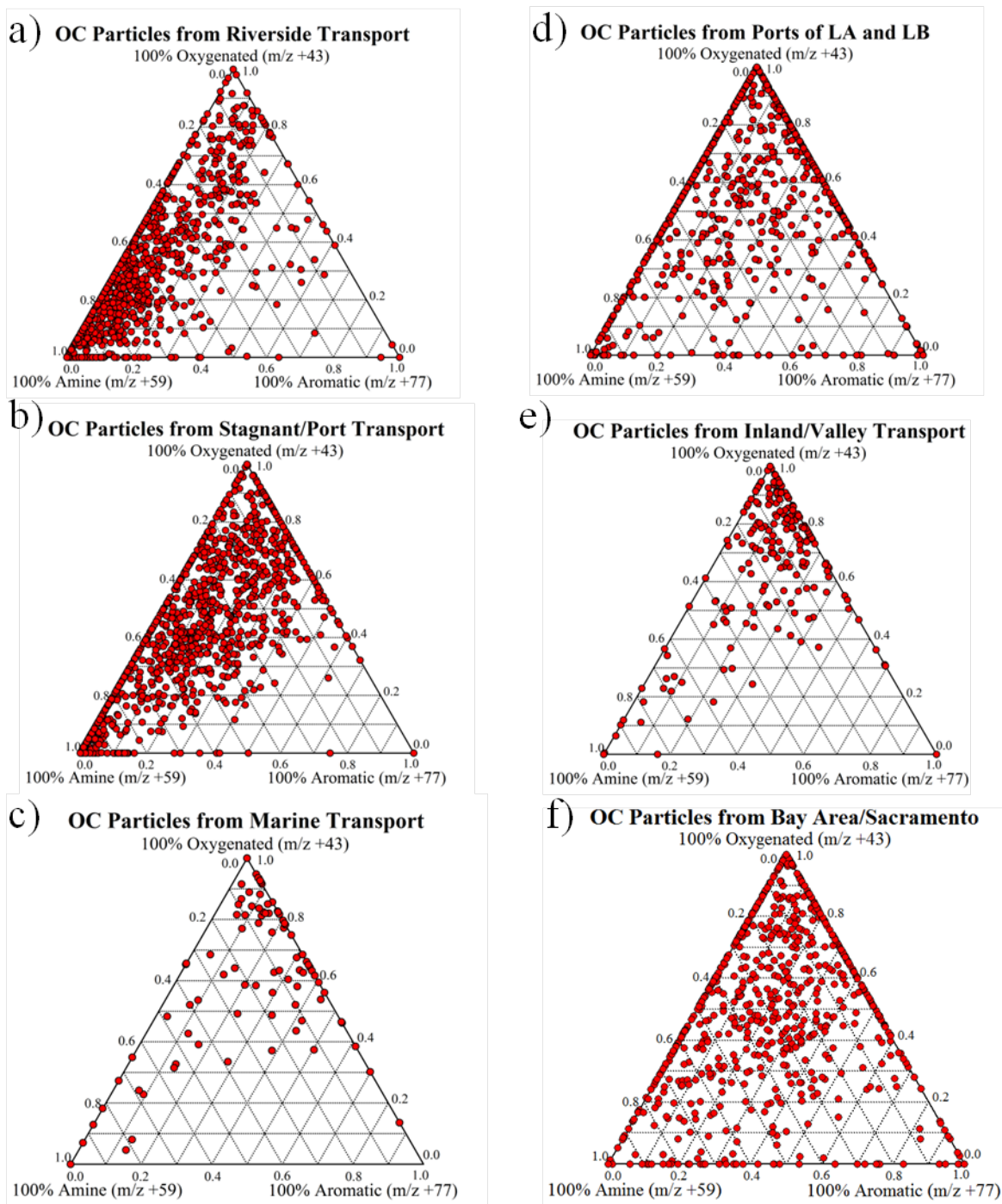
Figure 8: Ternary plots for individual OC particles observed for the 6 different time periods. The top corner of the ternary plots corresponds to OC particles containing only the oxygenated organic peak ($^{43}C_2H_3O^+$), the left bottom corner denotes OC particles containing only the amine

970   peak ($^{59}(CH_3)_3N^+$), and the right bottom corner corresponds to OC particles containing only the

971   aromatic peak ($^{77}C_6H_5^+$).

972
973
974
975
976
977